



Michigan Technological University  
**Undergraduate Research  
Symposium**

March 23, 2018



## Welcome to the 2018 Undergraduate Research Symposium!

The Undergraduate Research Symposium highlights the amazing cutting-edge research being conducted on Michigan Tech's campus by some of our best and brightest undergraduate students.

The students showcasing their work today have spent a significant portion of the past year working alongside Michigan Tech faculty and graduate students to explore, discover and create new knowledge. They've spent long hours in the lab or out in the field designing experiments, gathering data, creating new models and testing hypotheses. They've applied their classroom knowledge in new and sometimes unexpected ways, and developed new skills that will propel them forward in their careers.

Each of the presenters has been mentored by a faculty member who took great care to guide them through the rigors and exhilaration of pioneering research projects. They've shared in arduous tasks, brainstormed, adjusted hypotheses and regrouped as their projects have taken shape. Through the process, they've built strong relationships that will last a lifetime. The students presenting today represent a wide array of disciplines from across campus and highlight the diversity of research areas being explored.

I would like to take this opportunity to thank our partners and sponsors who have funded the work of many of the students that you will see on display today. In particular, I want to recognize the office of the Vice President for Research for funding the Summer Undergraduate Research Fellowship Program, as well as the Portage Health Foundation and the Michigan Space Grant Consortium for funding the Undergraduate Research Internship Program.

I sincerely hope that you enjoy visiting with our students and learning about their research endeavors today. Challenge them with your questions and experience the passion that is Michigan Tech!

Sincerely,



Lorelle Meadows  
Dean, Pavlis Honors College

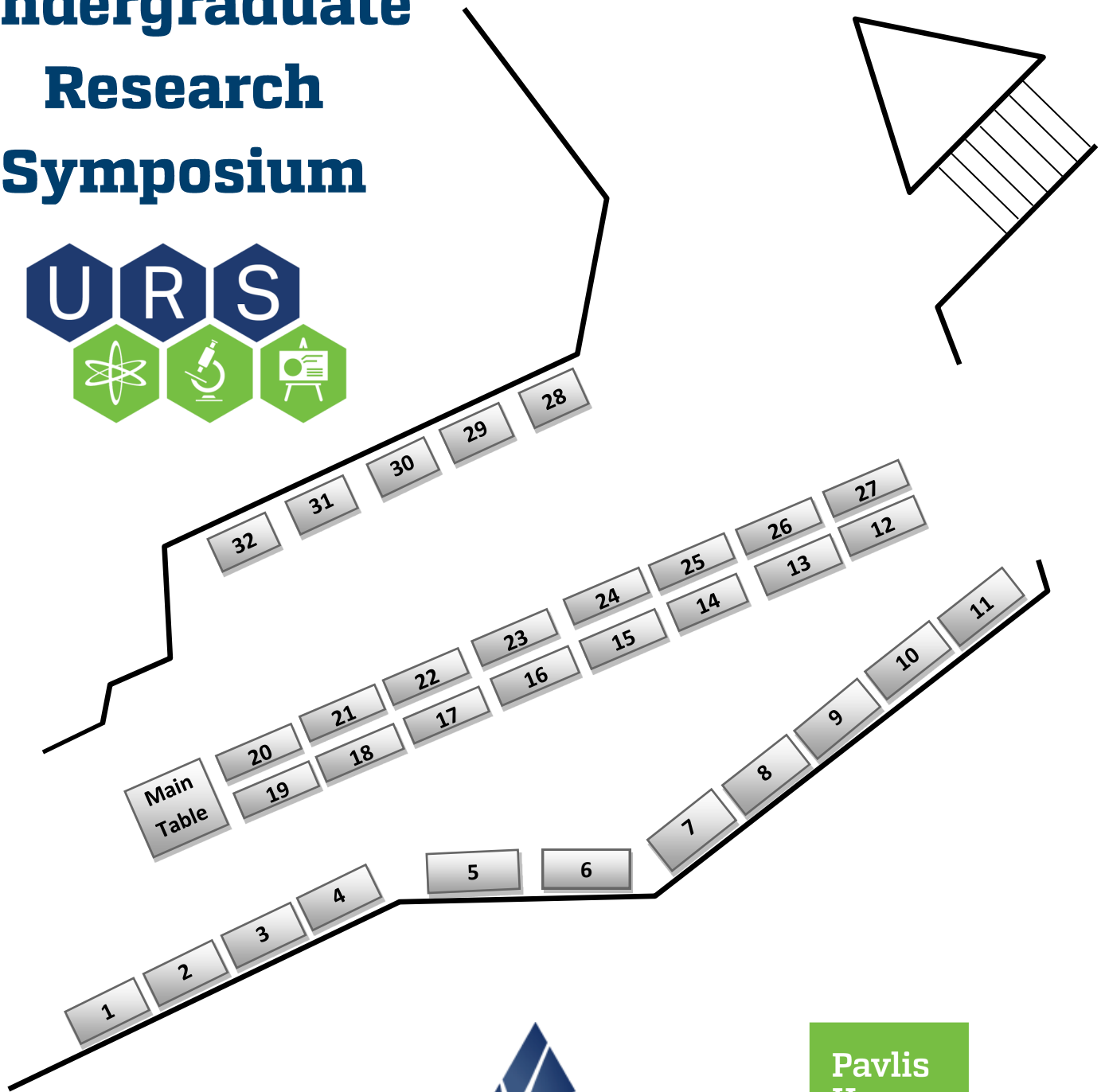


**Michigan Tech**

**Pavlis  
Honors  
College**



# Undergraduate Research Symposium



**SURF**



The Pavlis Honors College would like to welcome you to the 2018 Undergraduate Research Symposium!

The research presented here is sponsored in part by the Office of the Vice President of Research, the Portage Health Foundation, the Pavlis Honors College, and the Summer Undergraduate Research Fellowship program.

## SESSION A: 1-3 PM

	Presenter	Department	Title
1	Alex Baker	Civil and Environmental Engineering	Multiobjective Optimization of Cost and Strength for Various Lengths of Doubly Reinforced Concrete T-beams.
2	Alicia Ball	Mechanical Engineering - Engineering Mechanics	3D Bioprinting with Induced Pluripotent Stem Cells and Collagen I for Enhanced Differentiation to Cardiomyocytes
3	Stephanie Bedford	Mathematical Science	Estimating Intrinsic Dimension with Local and Global Approximations
4	Dale Bigler	Mathematics	Towers of Algebras Related to Symmetric Groups and Hecke Algebras
5	Elisabeth Billman-Benveniste	Chemistry	Effect of Molecular Contaminants on Polycarbonate Interfaces Addressed at the Quantum Chemical Level
6	Katelyn Buchalski	Civil and Environmental Engineering	Food-Energy-Water Nexus in Household Metabolism
7	Michelle Burge	Kinesiology and Integrative Physiology	Age-related Alterations in Muscle Function and Architecture of the Lower Limbs in Middle-aged and Young Women
8	Thomas Bye	Kinesiology and Integrative Physiology	Respiratory Muscle Fatigue Limits Upper-Body Exercise Tolerance in Collegiate Cross-Country Skiers
9	Hannah Cunningham	Kinesiology and Integrative Physiology	Total Sleep Deprivation and Pain Perception During Cold Noxious Stimuli in Older Adults
10	Savannah de Luca	Social Sciences	Digital Inventory of Historic Mineralogical Instruments at the A.E. Seaman Museum
11	Crystal Fletcher	Computer Science	Evaluating Input Strategies for Modulating Touchscreen Keyboard Decoding
12	Jacob Franz	Chemistry	Incorporating 3D Printed Molecular Models as Educational Aids in the STEM: A Step-by-Step Procedure for Educators and Students
13	James Gooding	Chemistry	Formation of Hindered Arylcarbamates using Alkyl Aryl Carbonates under Highly Reactive Conditions
14	Jennifer Hannon	Biomedical Engineering	Understanding the Importance of Physiologically Relevant Conditions in In Vitro Wound Models Using Fibroblasts
15	Amanda Kautzer	Biomedical Engineering	Comparison of Multi-arm PEG-based Hydrogels for Tendon and Ligament Repair

16	Ryan Kibler	Civil and Environmental Engineering	Using a property-carrying particle model for ecosystem simulation: a case study of Sandusky Bay
17	Abigail Kuehne	Cognitive and Learning Sciences	Cybersecurity Knowledge, Feelings, and Phishing
18	Sam Lakenen	Chemical Engineering	Development of an Open Source Roller Bottle Apparatus
19	Benjamin D. Miller	Forestry and Applied Ecology	Vertical gradients of leaf and air temperature in a tropical wet forest canopy
20	Anna Nelson	Chemical Engineering	Puffy Paint: A Novel Material for Microdevice Duplication
21	Elsa Schwartz	Forestry	Acclimation patterns of stomatal density and size in response to experimental warming and a vertical canopy gradient in four rainforest species
22	Benjamin Sovinski	Geological and Mining Engineering & Sciences	Simultaneous Simulation of Mineral Grades using Geostatistical Methods
23	Deanna Springgay	Chemistry	Peptide-Based Nanoparticle for Cancer Therapy
24	Rachel Stern	Environmental Engineering	Phosphorus Levels in Small Local Lakes
25	Drew Stockero	Visual and Performing Arts	Preserving the Upper Peninsula Through Soundscapes
26	Timothy Stone	Social Sciences	Doctor's Note: A Spatial Analysis of the Built and Social Determinants of Children's Health During the Copper Boom
27	Rose Turner	Environmental Engineering	Fate of Perfluorinated Compounds in Aqueous-phase Ultraviolet/Persulfate Advanced Oxidation Process
28	Brennan Vogl	Biomedical Engineering	Monitoring Migration of Cancer Cells Using a Microfluidic Device
29	Allison Waara	Kinesiology and Integrative Physiology	Aging and the Neurocognitive Mechanisms Underlying Corrective Actions for Obstacle Collision Avoidance
30	Kira Warner	Cognitive and Learning Sciences	Measuring Student Financial Literacy
31	Travis Wigstrom	Chemistry	Electronic Structure Investigations of Sulfenamide Form of Omeprazole in Interaction with the Primary Amino Acid Sites of H <sup>+</sup> /K <sup>+</sup> ATPase

# 1. Multiobjective Optimization of Cost and Strength for Various Lengths of Doubly Reinforced Concrete T-beams.

Student Presenter: Alex Baker, Civil Engineering

Faculty Advisor: Amlan Mukherjee, Civil & Environmental Engineering

**Introduction:** The purpose of this study is to explore tradeoffs of material cost and allowable distributed load in the design of reinforced concrete T-beams. To study these tradeoffs, multi-objective optimization was performed on beams of various lengths to obtain Pareto optimal designs. The resulting Pareto frontiers give decision-making power in deciding economical beam layouts and material choices while also providing optimal beam sections. Previous work has identified cost-optimal section designs, but have mostly neglected varying material properties, beam layouts, and loading, which are addressed in this study.

**Materials and Methods:** The optimization was performed with a genetic algorithm programmed in MATLAB which allowed all applicable variations in material and dimensional properties per American Concrete Institute (ACI) code 318. ACI-318 is the standard design specification for reinforced concrete structures. To generate the Pareto curves, a length was specified and the problem was treated as a multi-objective optimization problem to maximize the strength (allowable distributed load) while minimizing the cost. As the study deals with varying beam layout and loading, material properties were treated as variables. Constraints were implemented into the genetic algorithm so that each possible “genome” created beam geometries that stayed within the feasible solution space. This process eliminated the need for constraint checks and a penalty system within the algorithm, as used in previous research. The available distributed load was assessed by subtracting the self-weight moment of the beam from the sectional strength. It was then normalized to an area load on the T-beam. The concrete and steel costs were considered to assess the cost of the reinforced concrete beam. Models for both concrete and steel cost were formulated using previous literature and current industry metrics. The total was then normalized per unit area on the T-beam.

**Results and Discussion:** The result of the study is a graph displaying Pareto curves of cost/strength optimal section designs for various beam lengths. The graph will serve as a design aid to identify the trade-offs between the cost of increasing the loading and/or of changing the beam length in reinforced concrete beam design. Further analysis of the Pareto optimal beam designs can help to identify variable relationships such as ranges of loading and beam lengths in which certain concrete grades or steel grades are economical, or identifying LCA environmental impact curves. Additionally, modifications have been made to the prevailing algorithm to improve the method of handling constraints. Previously, penalty systems were implemented to eliminate section designs that violate the constraints, thus causing the algorithm to search the non-valid solution space. The proposed approach eliminates the need to check constraints by normalizing the independent variables within bounded dependent constraints. Hence, the algorithm only seeks solutions for section designs within the valid solution space. This approach was taken to handle the high number of variables and constraints in reinforced concrete beam design.

## 2. 3D Bioprinting with Induced Pluripotent Stem Cells and Collagen I for Enhanced Differentiation to Cardiomyocytes

Student Presenter: Alicia Ball, Chemical Engineering

Faculty Advisor: Parisa Abadi, Mechanical Engineering- Engineering Mechanics

**Introduction:** Heart disease is the number one killer in the United States. With the ability to reconstruct tissue and produce cells, such as the cardiomyocyte (CM) this disease can be counteracted. One way to do this is by bioprinting induced pluripotent stem cells (iPSCs) into a 3D structure and differentiating them to CM. We used Collagen I, which is the main structural protein found in skin and other connective tissues. When combined with iPSCs and alginate to form a bio-ink, it can be bioprinted and then used to conduct research for regenerative therapy and other possible forms of treatment.

**Materials and Methods:** Collagen I in dilute acetic acid solution was diluted to 2.5 mg/ml and neutralized using NaOH inside a sterilized laminar flow hood. Neutralized collagen kept at 5° C was combined with 4% weight alginate and iPSCs. The CAD program, SolidWorks, was used to create the desired shape of the construct which is then translated into G-code by the Allevi BioBot bioprinting software. The tricomponent collagen bio-ink was added to the syringe and attached to the BioBot and printed at 10 PSI. Our strategy uses a syringe pump with dual syringe ports that is used to print the bio-ink with a CaCl<sub>2</sub> cross-linking solution utilizing a co-axial syringe attached to the printer head that will simultaneously extrude cross-linker and bio-ink. After the structure is printed, iPSC containing 3D printed tissue is covered with stem cell culture medium and on day 4 differentiation of iPSCs to CM is begun using standard protocols. The main goals of this research are testing the viability of fragile iPSCs in collagen I based bio-inks, optimizing the mechanical strength of traditionally low viscosity collagen I by creating hybrid bio-inks, and enhancing iPSC differentiation to CM by providing a free-standing 3D matrix with complex geometry

**Results and Discussion:** Initial studies tested the viability of iPSCs in both a pure collagen I bio-ink as well as a collagen I/alginate bio-ink cross linked with CaCl<sub>2</sub>. Collagen I is a known slow gelling material at room temperature and thus has insufficient viscosity and solidity to maintain iPSCs in a 3D printed structure, as demonstrated in previous studies with other cell types. However, we found that when mixed with sufficiently high volume fraction of iPSCs the viscosity increased sufficiently to print a single layer which could be used for viability studies. We found that on day 4 post-seeding Calcein AM staining showed that iPSCs remain viable on floating gels of collagen I or collagen I/alginate demonstrating the viability of these materials to maintain iPSC adhesion and differentiation. Additionally, 2.5 mg/ml collagen I and 4% weight alginate could be printed into a lattice structure inside a 2% weight gelatin gel with 10 mM CaCl<sub>2</sub> cross linker demonstrating sufficient viscosity and solidity of the bio-ink to create complex geometries. Studies utilizing a co-axial needle to simultaneously print CaCl<sub>2</sub> solution and the bio-ink to create free standing and robust tissue structures are that main goal of this research and are on-going.



### 3. Estimating Intrinsic Dimension with Local and Global Approximations

Student Presenter: Stephanie Bedford, Applied Mathematics and Computation  
Faculty Advisor: Dr. Ben Ong, Mathematical Sciences

**Introduction:** In the field of exploratory data analysis, intrinsic dimension is a core topic for analyzing data sets of high dimension. The intrinsic dimension of a given data set estimates the lowest number of variables needed to describe the data. These estimations are important in data modeling, and insure minimal loss of data. In this poster, we will explore many popular estimators of intrinsic dimension. We will research how these six methods perform on generated and real data sets, comparing accuracy, precision, and accessibility of each.

**Materials and Methods:** (local approximation) We will use nearest neighbor approach to estimate the intrinsic dimension based on the average distance from a data point  $x$  to the  $k$ -th neighbor of  $x$ . The correlation dimension is the assumption that the number of observations in a hypersphere of radius  $r$  is proportional to  $r^d$ , where  $d$  is the intrinsic dimension. In the maximum likelihood approach, instead of directly computing the correlation dimension. Specifically, we will model  $x(i) = g(y(i))$ , and count  $N_x(t)$  the number of observations within distance  $t$  from  $x$ . For estimation using Packing Numbers we will find the smallest number of hyperspheres with radius  $r$  that are needed to cover all observations in the data set by plotting the difference of  $\log(r_i)$  against  $\log(r_j)$  for  $i$  not equal to  $j$ .

(global approximation)

We will estimate intrinsic dimension using PCA by finding the integer  $k$  such that  $\sum(s(i), i=1..k) \leq 0.9 * \sum(s(i), i=1..n)$ , where  $s$  are the singular values of the data.

We will use the spectral gap (comparing ratios of  $s(i)/s(i+1)$ ) to estimate the intrinsic dimension.

**Results and Discussion:** We will research how these six methods perform on generated and real data sets, comparing accuracy, precision, and accessibility of each. We hope to identify the global estimator that performs best on the generated data sets, and a local estimator that performs best on a majority of the generated data sets. We will also use real data sets from the Santa Fe time series competition, to see how our estimates for intrinsic dimension compare to nearly exact solutions for dimension.

Ben Fulcher, Max Little, Nick S. Jones. Highly comparative time-series analysis: The empirical structure of time series and their methods. *Journal of the Royal Society Interface* 10: 20130048.

## 4. Towers of Algebras Related to Symmetric Groups and Hecke Algebras

Student Presenter: Dale Bigler, College of Sciences and Arts  
Faculty Advisor: Jie Sun, Mathematical Sciences

### Introduction:

In a recent paper, Savage and Yacobi defined a tower of algebras to be a graded algebra which satisfies four axioms. Under additional conditions, the Grothendieck groups of the categories of finitely generated left modules and finitely generated projective left modules over a tower of algebras can form a dual pair of Hopf algebras. Examples of such towers of algebras include the tower of group algebras of symmetric groups  $\mathbb{C} \oplus \mathbb{C} \oplus \mathbb{C} \oplus \dots$  and the tower of 0-Hecke algebras  $H_n(0)$ .

**Materials and Methods:** Not available

### Results and Discussion:

We prove that the graded algebra  $H \oplus H \oplus H \oplus \dots$ , introduced by Hivert and Thiery, also satisfies the axioms of a tower of algebras. In particular,  $H \oplus H \oplus H \oplus \dots$  is a two-sided projective  $H \oplus H \oplus H \oplus \dots$ -module

## 5. Effect of Molecular Contaminants on Polycarbonate Interfaces Addressed at the Quantum Chemical Level

Student Presenter: Elisabeth Billman-Benveniste, Chemistry

Faculty Advisor: Dr. Loredana Valenzano-Slough, Chemistry

**Introduction:** This project employed state-of-the-art quantum mechanical methods including Density Functional Theory (DFT) to address interactions between polycarbonate interfaces and water molecules. Polycarbonates are thermoplastic materials that exhibit optical transparency and high impact resistance, elasticity, and scratch resistance. Their mechanical properties have been exploited to create scratch resistant coatings for electronic screens and eyeglass lenses, and extensively in bulletproof glass. The interaction of atmospheric contaminants with polycarbonates are of major concern to manufacturers and consumers alike, as such interactions have the potential to change the chemical structure, stability, and the mechanical properties of polycarbonates.

**Materials and Methods:** The quantum chemical Gaussian09 software package was used to build and relax the structures of numerous polycarbonate models varying in size and complexity. The stability of the numerical solutions were tested by performing frequency calculations which, in addition, allowed for determination of vibrational spectra and thermochemical information such as enthalpy, entropy, and Gibbs free energy. These calculations, performed in absence of contaminants (i.e., in vacuum), provided a comparative reference base to address changes in the behavior of the material with respect to its interaction with water molecules. The accuracy of the results were benchmarked using several levels of theory (DFT functionals) including methods able to account for the long-range forces expected to play a determining role in the water/polycarbonate interactions.

**Results and Discussion:** Geometry relaxation calculations were successfully performed to determine the most energetically stable form of four polycarbonate models: a monomer, dimer, trimer, and tetramer of the linear polymeric structure. On such structures, water molecules were added in a step-wise fashion to each of the polycarbonate model. In the case of the monomer, two water molecules were introduced: (i) one to interact through the hydrogen atom with the double-bonded oxygen of the carbonate group; (ii) the second one to interact through the hydrogen atom with one of the benzene rings of the monomer. The same approach was repeated for the polycarbonate dimer, trimer, and tetramer models. In all cases, Hess's Law was applied to determine the strength of the guest/host interactions. The main conclusion drawn was that water molecules preferentially interact with the double-bonded oxygen in the carbonate structure of the polycarbonate molecule as opposed to its benzene rings. As such, this conclusion sets the foundation for future, more sophisticated investigations able to assess changes of the polycarbonate structure and the resulting effect on the mechanical properties of the material.

## 6. Food-Energy-Water Nexus in Household Metabolism

Student Presenter: Katelyn Buchalski, Environmental Engineering  
Faculty Advisor: Dr. Daisuke Minakata, Civil & Environmental Engineering

**Introduction:** A rapid increase in global population and economic growth presents critical challenges to a sustainable future, including renewable technologies, sustainable agriculture production practices, and advancing water reuse. The widespread adoption of these solutions could take a tremendous amount of time. In response to this time variable, there is growing evidence that conservation and demand-side approaches warrant greater attention for tackling with a food-energy-water (FEW) nexus approach. Making small changes to household appliances and introducing greywater systems could produce great environmental impacts including the amount of energy and water consumed as well as CO<sub>2</sub> emitted.

**Materials and Methods:** I am tasked with finding FEW technological options and scenarios that would be implemented into a household system. Data is obtained for national levels of water and energy usage based on a 3-person household. The first step of the project is to go through the effects of one upgraded household technological option. The technological option is analyzed to determine its energy and water efficiency as well as black and grey water treatment processes. Different amounts of water treatment steps are analyzed for black and grey water, ranging from a membrane bioreactor to a combination of membrane bioreactor, UV disinfectant, and sedimentation. The FEW nexus is referenced to visualize the distribution of now surplus water and energy from the upgraded technological option.

**Results and Discussion:** The upgraded toilet options include low flush with gravity sewers, vacuum, urine diverting and conventional low flush. All the upgraded toilets provide at least a 75% decrease in water consumption when compared to a conventional toilet. The water coming into and from this system is analyzed and compared to potable water and grey water entering the system. Also, when grey water goes through the water treatment process, it undergoes a heat exchange and is captured and then applied to the heat pump for water heaters in the household. The FEW nexus for an average household can then be applied to the national levels of energy and water consumption and the effects of recycling energy and water with more efficient technological options can be compared visually. It is critical that the population starts to understand and apply sustainability practices since time is a developing variable.

## 7. Age-related Alterations in Muscle Function and Architecture of the Lower Limbs in Middle-aged and Young Women

Student Presenter: Michelle Burge, Exercise Science  
Faculty Advisor: Dr. Tejin Yoon, Kinesiology/Integrative Physiology

**Introduction:** The age-related declines in muscle mass and functions are greater for women and the lower limb muscles. However, it is less clear which lower limb muscles may be compromised more in middle-aged women. Therefore, the purpose of this study was to compare muscle function and architecture of the knee extensors and plantar flexor muscle in young and middle-aged women.

**Materials and Methods:** Twenty-two middle-aged ( $54 \pm 6$  yr) and 17 young women ( $21.8 \pm 1.4$  yr) volunteered to participate in this study. In vivo muscle architecture measurements such as muscle thickness and pennation angle of four muscles including vastus lateralis (VL), rectus femoris (RF), Gastrocnemius medialis (GM) and lateralis (GL) were measured using a B-mode real-time ultrasound scanner. Each participant performed maximal voluntary isometric contractions (MVIC) of knee extensor and plantar flexor muscles 3-4 times on the Biodex dynamometer. Additionally, the 6-minute walk test and sit-to-stand task were performed. Independent t-tests were used to examine the age-related differences.

**Results and Discussion:** The middle-aged women had significantly lower MVIC torque of the quadriceps ( $119.0 \pm 19.5$  Nm vs.  $169.0 \pm 51.7$  Nm,  $p < 0.001$ ) and plantar flexor muscles ( $109.0 \pm 30.6$  Nm vs.  $140.0 \pm 49.4$  Nm,  $p < 0.05$ ) compared to young women. Thickness of the GM was similar between groups, however, thickness of all other muscles were significantly greater for the young women ( $p < 0.01$ ). Pennation angles were similar between groups for the quadriceps muscles, while significantly greater values were noted for the plantar flexor muscles in the young women ( $p < 0.05$ ). Performance of the 6-minute walk was similar between groups; however, the middle-aged women performed significantly fewer repetitions during the sit to stand task ( $18.0 \pm 4.9$  vs.  $25.0 \pm 6.7$  reps,  $p < 0.001$ ). These results suggest that declines in strength, muscle architecture and functional performance are already apparent by middle age in women. Strengthening interventions of the legs should be considered to delay muscle atrophy and functional declines in middle-aged women.



## 8. Respiratory Muscle Fatigue Limits Upper-Body Exercise Tolerance in Collegiate Cross-Country Skiers

Student Presenter: Thomas Bye, Exercise Science

Faculty Advisor: Dr. Steven Elmer, Kinesiology and Integrative Physiology

**Introduction:** The development of respiratory muscle fatigue compromises lower-body exercise performed to the limit of tolerance, especially in endurance athletes. It is unclear if respiratory muscle fatigue has a similar effect on upper-body exercise tolerance where respiratory muscles have important respiratory, postural, and locomotor roles. The purpose of this study was to evaluate the effects of inspiratory muscle fatigue on upper-body exercise tolerance. I hypothesized that high-intensity arm cranking performed by upper-body endurance trained athletes would induce considerable ventilator stress and reduce upper-body exercise tolerance.

**Materials and Methods:** Seven male Division I collegiate cross-country skiers ( $20 \pm 2$  yrs,  $183 \pm 6$  cm,  $76 \pm 6$  kg, upper-body  $VO_{2peak}$  and  $W_{peak}$   $50 \pm 5$  mL/kg/min,  $197 \pm 24$  W, respectively) performed two upper-body exercise trials. For the control exercise trial (CON-EX), athletes performed arm-cranking at  $\sim 85\%$  of  $W_{peak}$  ( $170 \pm 20$  W) until their limit of tolerance. For the inspiratory muscle fatigue exercise trial (IMF-EX), athletes performed the same task while having pre-existing fatigue in their inspiratory muscles ( $\sim 20\%$  reduction in maximal inspiratory pressure) induced through a threshold resistance breathing device. Physiological responses and the limit of tolerance were compared between trials.

**Results and Discussion:** During CON-EX, ventilatory demand was high as indicated by the high ventilation rates ( $137 \pm 17$  L/min). After CON-EX, MIP decreased by  $10 \pm 8\%$  ( $158 \pm 30$  vs.  $136 \pm 26$  cm H<sub>2</sub>O) and remained reduced by  $7 \pm 7\%$  for 11 min ( $P < 0.05$ ). Compared to CON-EX, IMF-EX limit of tolerance decreased by  $33 \pm 14\%$  ( $14.2 \pm 2.4$  vs.  $9.6 \pm 2.7$  min,  $P < 0.01$ ). During IMF-EX, ventilation, breathing frequency, perceived exertion, and dyspnea increased whereas tidal volume decreased (all  $P < 0.05$ ). For these collegiate cross-country skiers, high-intensity arm-cranking taxed their respiratory muscles and impaired their inspiratory muscle function. Further, artificial induction of inspiratory muscle fatigue decreased limit of tolerance and increased perceptual stress. Collectively, our results demonstrate the functional consequences of inspiratory muscle fatigue on upper-body performances. Our findings of increased ventilatory stress and reduced upper-body exercise tolerance in athletes who regularly performed upper-body endurance exercise contrasts previous upper-body research using untrained individuals. Thus, further research is needed to explore the impact of respiratory muscle fatigue has on upper-body performance and the mechanisms behind it. These findings have implications for athletes performing upper-body exercise, researchers, and clinicians.

## 9. Total Sleep Deprivation and Pain Perception During Cold Noxious Stimuli in Older Adults

Student Presenter: Hannah Cunningham, Biomedical Engineering  
Faculty Advisor: Jason Carter, Kinesiology/Integrative Physiology

**Introduction:** A bidirectional relationship exists between sleep deprivation and pain, and perceived pain has been positively correlated with increased sympathetic nerve activity. Understanding the relationship between sleep, perceived pain and muscle sympathetic nerve activity (MSNA) is critical to develop cost effective strategies for the management of pain. We hypothesized that 24-hour total sleep deprivation (TSD) would increase pain perception to cold noxious stimuli in older men and women, and increased pain perception would be augmented in postmenopausal women when compared to age matched men.

**Materials and Methods:** We examined the effects of 24-hour TSD on perceived pain and MSNA during a 2-minute cold pressor test (CPT). Testing was carried out in 10 postmenopausal women ( $61 \pm 2$  yrs,  $26.4 \pm 1.4$  BMI) and 10 age-matched men ( $60 \pm 1$  yr,  $27.2 \pm 0.8$  BMI). All subjects reported to be nonsmokers with no history of cardiovascular disease, autonomic dysfunction, asthma, or diabetes. Trial order was randomized, and testing sessions of normal sleep (NS) and TSD were separated by approximately one month. Nerve recordings were collected through microneurography of the subject's right peroneal nerve. For two minutes, subjects immersed their left hand, up to the wrist, in an ice water bath ( $\sim 1^{\circ}\text{C}$ ), and perceived pain was recorded every 15 seconds from a modified Borg scale (6-20 arbitrary units a.u.). MSNA was recorded throughout the session and averaged for each 15 second interval.

**Results and Discussion:** Perceived pain responses were augmented following TSD. This was observed when perceived pain was expressed as a mean (NS  $\Delta 6.9 \pm 2.4$ , TSD  $\Delta 8.2 \pm 2.4$  a.u.;  $p < 0.05$ ) and as a peak (NS  $\Delta 8.4 \pm 2.7$ , TSD  $\Delta 9.7 \pm 2.5$  a.u.;  $p < 0.05$ ). Consistent with findings in a younger population (Larson and Carter, 2016), TSD significantly increased pain, but there were no significant sex differences. Peak pain was not correlated to MSNA responsiveness, suggesting a secondary stimulant acting on perceived pain. In summary, TSD increases pain perception during cold noxious stimuli to a similar extent in postmenopausal women and age-matched men.



## 10. Digital Inventory of Historic Mineralogical Instruments at the A.E. Seaman Museum

Student Presenter: Savannah de Luca, History - Social Sciences

Faculty Advisor: Dr. Steven Walton, Social Sciences & Dr. Andrew Fiss, Humanities

**Introduction:** Prior to this research, the A.E. Seaman Mineral Museum had basic cataloging data for some of their antique instruments, but has done no thorough study of any and no synthetic comparison of them all. The instruments catalogued during this research became a significant portion of the Inventory of Historic Scientific Instrument (IHSI) database at Michigan Tech, (see [ihsi.omeka.net](http://ihsi.omeka.net)). A collection of historical mineralogical instruments has great educational and research value potential, a potential that cannot be achieved without proper documentation (Holland 1999). This research has provided this documentation and told the story of the history of geological instrumentation in the Keweenaw Peninsula.

**Materials and Methods:** In order to create factual and complete entries in the IHSI database, Dr. Christopher J. Stefano, Associate Curator of the A.E. Seaman Mineral Museum provided access to all antique scientific instruments, many were never cataloged by the museum prior to 2017. Each instrument was carefully assessed through measurement, observation, and photography. The data collected was associated to several fields in two separate spreadsheets. Sheet 1 contained the fields: Photograph Number, Catalog Number, Object Photos, Physical Dimensions, Materials, Inscription, Scale, Notes, and Catalog Number Added. Sheet 2 contained the fields associated with the IHSI database entries. Multiple photographs of each entry were taken using a Canon EOS 30D DSLR camera, black fabric background, and two tripods set up within the storage room of the museum. They were edited using iPhoto software. Once uniform, a batch upload of sheet 2 was then performed in order to efficiently create entries in the online database. Both the physical and functional descriptions of each item were then written using several primary sources from the A.E. Seaman Mineral Museum, as well as online secondary sources. These descriptions, as well as the final edits of photographs, were then uploaded onto the IHSI database, completing the entries.

**Results and Discussion:** The first comprehensive catalog of antique scientific instruments located at the A.E. Seaman Mineral Museum now consists of 71 entries in the Inventory of Historic Scientific Instruments database. Each entry is complete with multiple finished photographs, and all data collected includes the name of object, subject, physical and functional descriptions, original date or estimated original date, language, physical dimensions, materials, inscriptions, scales, maker, and location. Of the 71 instruments recorded in the IHSI database, 12 of these items received a museum catalog number for the first time. These 12 items were then entered into the Mineral Museum's database by Dr. Christopher J. Stefano, allowing for a more comprehensive picture of the contents of the museum. Many of these objects were previously unidentified objects, including the Starett Surface Gage, multiple petrographic microscopes, and various microscope lenses or parts. Through this research, these instruments were able to be identified and their descriptions have been added to both the museum database as well as the IHSI database.

# SURF

# 11. Evaluating Input Strategies for Modulating Touchscreen Keyboard Decoding

Student Presenter: Crystal Fletcher, Computer Science  
Faculty Advisor: Keith Vertanen, Computer Science

**Introduction:** Input using onscreen virtual keyboards normally consists of a sequence of tap events that specify some amount of text, usually a single word. But is single word-at-a-time entry the best choice? Our study compared the entry and error rates of users entering text via word-at-a-time, multiple-word-at-a-time, and sentence-at-a-time strategies. Virtual keyboard typing is typically aided by an auto-correct method that aims to decode a user's taps into their desired input but sometimes makes mistakes. Our study also explored a technique we call letter locking that gives a user the ability to prevent the decoder from changing a certain keypress.

**Materials and Methods:** We conducted two experiments, each with two parts. In the first experiment, participants were asked to type a set of phrases on a smartwatch virtual keyboard either one-word, two-words, or an entire sentence-at-a-time. Input was segmented by users swiping right to indicate a space and request recognition from the decoder. All trials from each strategy were presented together, but the order in which the strategies were presented was varied between participants. They were then asked to compose their own phrases using whichever input strategy they preferred. In the second experiment, participants were asked to complete two sets of phrases, one with our lock letter feature and one without. The order of these sets was again varied between participants. Participants were then asked to compose their own phrases on the smartwatch using the lock letter feature and enter the phrase they intended to type on a laptop.

**Results and Discussion:** Our findings suggest virtual keyboards can enhance performance by encouraging users to provide more input per recognition event, and show that letter locking further reduced error rates for both transcription and composition tasks. Additionally, we contribute a new phrase set with more difficult to predict words and present a new composition-based method for evaluating text entry methods. The results of our experiment suggest two design implications. First, recognition-based touchscreen input methods should be designed to allow users to modulate the amount of input per recognition event. Second, letter locking is a simple, easy-to-use, and easy-to-understand technique that results in substantial reductions in error rate at a modest reduction in entry rate.

## 12. Incorporating 3D Printed Molecular Models as Educational Aids in the STEM: A Step-by-Step Procedure for Educators and Students

Student Presenter: Jacob Franz, Mechanical Engineering  
Faculty Advisor: Dr. Loredana Valenzano-Slough, Chemistry

**Introduction:** Throughout the past few years, the popularity of 3D printing has literally exploded. Hundreds of technological advancements have transformed the world of 3D printing from cumbersome and costly to efficient and highly profitable, and have seen industrial and academic organizations implementing methods as invaluable modeling tools. In this work, we present an in-depth, step-by-step procedure for the conversion of virtual molecular structures to 3D-printable, physical models that can be easily used in both research and class environment. The project, thought as an accessible and low-cost service for schools, educators, and students at all levels, strictly adheres to the open-source philosophy.

**Materials and Methods:** This project was conducted on personal computers with a minimum of 2 GB of RAM and a 32-Bit Dual Core 2GHz CPU. Following the open-source approach, several free 3D-modeling and printing software programs were utilized. These are: (i) Chimera, used to view and convert protein database (PDB) files into stereolithography (STL) or virtual reality modeling language (VRML) format; (ii) Blender, used to split chemical structures or adjust the smoothness of the molecular models; and, (iii) a combination of Slic3r Prusa Edition and Cura Lulzbot Edition, used to prepare STL files to be exported and printed, respectively. All molecular models were printed using a Lulzbot Taz 5 3D Printer and polylactic acid (PLA) filament. Care was taken to ensure that the print bed was properly calibrated and sufficiently leveled. In addition, to ensure consistency in the quality of the final products, the polyetherimide (PEI) print surface of the 3D printer was cleaned with isopropyl alcohol prior to each print. Finally, appropriate tools such a clam knife, paint scraper, X-Acto Knife, safety glasses, pliers, and flush cutters were utilized to remove the 3D models and any added support material from the printer bed.

**Results and Discussion:** The major outcome of this work is a detailed self-consistent procedure to efficiently and accurately manufacture 3D-printed molecular models. Through the use of multiple programs, the customization and modification of the final 3D models are enhanced. For example, our method allows for the 3D printing of molecular structures while maximizing their assembling and disassembling procedure, features that can be of particular interest for outreach activities involving students and audiences of all ages. Such capabilities are also suitable to a higher education environment, with the visualization of 3D-printed structures that can be used to visualize abstract concepts in other STEM disciplines, from math to physics, from chemistry to materials science and engineering. In addition, the outlined procedure has the capability of printing a wide range of molecular structures ranging from the simplest ones (single atoms and diatomic molecules) to more and more complex ones (amino acid chains, polymeric structures, crystalline models). As tangible 3D objects, molecular models are powerful tools in both academia and industry, as they provide an easy way to visualize abstract concepts and non-intuitive chemical structures. The procedure outlined in this project has the capability of producing such molecular models in a more customizable, efficient, and economical fashion.

### 13. Formation of Hindered Arylcarbamates using Alkyl Aryl Carbonates under Highly Reactive Conditions

Student Presenter: James Gooding, Chemical Engineering

Faculty Advisor: Dr. Shiyue Fang, Chemistry

**Introduction:** The most common reagent used to introduce them to amines is di-tert-butyl dicarbonate (commonly known as “Boc anhydride”) to obtain tert-butyl carbamates. The conditions are stirring the substrate amine with Boc anhydride in a mildly basic solution at room temperature. Due to the difficulty of synthesizing more complex carbonates with higher molecular weights, this approach cannot be employed to obtain other tertiary carbamates. The most widely used method to overcome this problem in the literature is to react an isocyanate with an alcohol. However, preparation of isocyanate needs an additional step and is usually difficult. In addition, stronger bases such as butyl lithium have to be used to abstract the proton of the alcohol for the reaction to occur. These conditions may not be compatible with many substrates. In some other cases, a strong base is not used, but harsh conditions such as high temperature and long reaction times are needed. These conditions may lead to unexpected rearrangements and side products.

**Materials and Methods:** Reacting an amine with a strong base before reacting it with a synthesized carbonate generates the protected amine without the drawbacks of the previous methods. A total of thirty-eight products were made using two carbonates and nineteen amine derivatives.

**Results and Discussion:** Yields for the products made vary from 26% to 78%. This new method for the protection of amines via the formation of tertiary, primary and secondary carbamates provides advantages over known carbamation methods. The new method can avoid the usage of difficult to prepare high molecular weight dicarbonates, sensitive isocyanate, catalysts, and high temperatures.

**SURF**

## 14. Understanding the Importance of Physiologically Relevant Conditions in In Vitro Wound Models Using Fibroblasts

Student Presenter: Jennifer Hannon, Biomedical Engineering  
Faculty Advisor: Dr. Smitha Rao, Biomedical Engineering

**Introduction:** Nitric oxide (NO) is a signaling molecule that is involved in immune modulation, extra cellular matrix production, promotes angiogenesis and works as an antibacterial agent. Studies have shown that it is involved in wound healing, although the exact time and duration of NO needed at the different stages of wound healing is unknown.

**Materials and Methods:** A device has been previously developed to measure the NO released from different cells in real time under physiological and pathological conditions.

**Results and Discussion:** If the amount of NO under physiological conditions is known, it can then be compared to how much NO is produced in a diabetic state (hyperglycemic). If it is found that NO production is low in hyperglycemic conditions, and it is known how much NO fibroblasts cells produce in normoglycemic conditions, the same amount of NO can be delivered in a hyperglycemic state. With the knowledge of how much NO is released by fibroblasts in physiological and hyperglycemic conditions, it can be used to link the different roles that NO plays in wound healing. This in turn could potentially facilitate the faster healing of diabetic foot ulcers.

# 15. Comparison of Multi-arm PEG-based Hydrogels for Tendon and Ligament Repair

Student Presenter: Amanda Kautzer, Biomedical Engineering, Mechanical Engineering  
Faculty Advisor: Rupak Rajachar, Biomedical Engineering

**Introduction:** Tendon and ligament tissues are often subjected to damage due to chronic overuse that gradually weakens the tissue at a microscopic level. Currently, the most common approach to healing these types of connective tissue injuries is rest and icing to minimize the effect of inflammation. Surgical approaches can also be used to attempt repair of these chronic injuries, but are often invasive and create a risk of further complications. As a less invasive alternative, injectable hydrogels can be used to mechanically support damaged tissues, as well as deliver therapeutic factors directly to the affected area to promote healing. These hydrogels, formed with poly(ethylene-glycol), or PEG, combined with fibrin(ogen), are vehicles to promote tissue stability and deliver therapeutic agents for soft tissue repair. The aim of this work is to characterize and compare the properties of gels formed from 4- and 8-arm PEG molecules with the goal of creating an injectable hydrogel that is customizable depending on the patient and injury type.

**Materials and Methods:** PEG and fibrinogen are separately dissolved into balanced phosphate buffered saline (PBS) solution at pH 7.4. Then the two solutions are mixed together to form a PEG-fibrinogen hydrogel matrix through crosslinking. Gels were analyzed using the following metrics: 1) curing time; 2) swelling ratio; 3) time dependent mechanical stiffness 4) degradation rate. Curing (gelation) time was measured using a simple tip test. Gels were considered cured when they ceased flowing in an inverted vial. Swollen weight ( $W_s$ ) was measured after 48 hours of incubation in PBS solution. Swelling ratio ( $Q$ ) was estimated by the swollen weight ( $W_s$ ) divided by the original dry weight ( $W_d$ ) of each sample ( $Q = W_s/W_d$ ). Rheometric data was taken with a TA Discovery HR-2 hybrid rheometer with an 8mm parallel flat plate to determine loss and storage modulus. Since the cross-linking process can significantly change stability of a hydrogel, the degradation behavior of the hydrogels in aqueous media was examined. Hydrogels were weighed prior to incubation in PBS, and a set of  $n = 3$  samples were removed at time periods  $t = 0, 3, 7, 14, 30$  days. Samples were freeze dried and the mass loss at each time-point was calculated. 8-arm PEG-fibrinogen hydrogels were compared with a control of 4-arm PEG-fibrinogen hydrogels

**Results and Discussion:** 8-arm hydrogels cured significantly faster than 4-arm controls [ $56 \pm 1.2$  and  $85 \pm 4.2$  seconds respectively]. The swelling ratio of the 8-arm gels was also significantly lower than 4-arm controls ( $1.02 \pm 0.02$  and  $0.87 \pm 0.01$  respectively) suggesting that increased crosslinking lowered the volume of aqueous solution permeating gels. Rheometric analysis showed that the 8-arm gels have a higher storage modulus than the 4-arm controls. And lastly, ongoing assessment of the degradation behavior suggests 4-arm gels degrade faster than the 8-arm gels.

# SURF

## 16. Using a property-carrying particle model for ecosystem simulation: a case study of Sandusky Bay

Student Presenter: Ryan Kibler, Environmental Engineering  
Faculty Advisor: Pengfei Xue, Civil & Environmental Engineering

**Introduction:** Situated on Lake Erie's southwestern shore in Ohio, Sandusky Bay is bordered by Ottawa, Sandusky, and Erie counties. This area is a mainstay to the northern Ohio economy because of its tourism and fishing industry. Today, approximately 80% of the Sandusky River watershed is devoted to agricultural purposes, thus loading the river with high concentrations of phosphorus. With the high loads of phosphorus, algae can utilize the nutrient and grow very quickly producing algal blooms.

**Materials and Methods:** To date, hydrodynamic modeling of Sandusky Bay is relatively limited; we have developed a high-resolution FVCOM model for this region. In this work, we will utilize a new technique which considers hydrodynamic effects and biological processes by integrating a property-carrying particle model (PCPM) and an Eulerian concentration biological model for ecosystem modeling.

**Results and Discussion:** Results show the integration of Lagrangian and Eulerian approaches allows for a very natural coupling of mass transport (represented by particle movements and random walk) and biological processes in water columns, which is described by a common vertical 1-D biological model. This method is considered to be far more efficient than traditional tracer based Eulerian bio-physical models for 3-D simulation, particularly for a large size of ensemble simulation.

## 17. Cybersecurity Knowledge, Feelings, and Phishing

Student Presenter: Abigail Kuehne, Communication, Culture, and Media and Psychology

Faculty Advisor: Dr. Adam Feltz, Cognitive & Learning Sciences

**Introduction:** The world's communication has increasingly involved the internet for dissemination of information. The resulting threats to privacy and security cost billions of dollars in internet crime and identity theft. While most Cybersecurity efforts are technical (i.e., hardware and software), my research attempts to understand one of these threats: susceptibility to phishing. Taking a human factors approach, I first developed an instrument to measure phishing susceptibility using real phishing emails; then predicted phishing susceptibility with a newly created Cyber-security knowledge scale; and finally, created phishing specific guilt and shame scales to measure motivations to pursue corrective actions after being phished.

**Materials and Methods:** Since the dispositions, attitudes, and cognitive abilities of end users are an under-explored impact of safe cyber practices, the first step in the project was to develop materials measuring the key outcome variable (phishing susceptibility) and main independent variables (e.g., Cyber-security knowledge) because they principally do not exist. I used Item Response Theory (IRT) to create a new phishing susceptibility scale and phishing knowledge scale. IRT techniques are often better than classical testing theory because they allow estimating item-level properties (i.e., discrimination and difficulty). Factor analytic techniques were used to develop instruments that measured how one would feel after being phished (i.e., guilty or ashamed). Then, after creating these instruments, I planned on using correlational techniques to predict key dependent variables. I chose two samples: one that roughly approximates the general U.S. population ( $N = 233$ ), and one of college undergraduates to determine if Phishing Knowledge and Cybersecurity knowledge increased through being a college student (i.e., higher education) ( $N = 159$ ).

**Results and Discussion:** My main predictions were supported by the data. The Phishing Susceptibility Scale, Phishing Knowledge scales, and Feelings after Being Phished scales achieved conventional levels of fit. As predicted, knowledge of Cybersecurity was a predictor of correctly identifying phishing emails ( $r = .42, p < .001$ ). Cybersecurity knowledge was higher in college samples than in the general population (Welch's  $t = 1.82, p = .04$  (one tailed),  $d = 0.18$ ). Cybersecurity knowledge was associated with higher feelings of phishing specific guilt ( $r = .27, p < .001$ ) and lower levels of cybersecurity phishing specific shame ( $r = -.29, p < .001$ ). These results contribute to the importance of education about cybersecurity. Increased knowledge of cybersecurity resulted in lowered risk of being phished; increased Cybersecurity knowledge also was associated with the positive emotion of guilt and negatively related to the undesirable emotion of shame. Guilt motivates one to take corrective action whereas shame motivates to take no action. Subsequently, Cybersecurity knowledge appears to be educable since a college sample was more knowledgeable than the general population. Future work is concentrating on predicting actual phishing attacks and developing educational interventions to increase Cybersecurity knowledge.

## 18. Development of an Open Source Roller Bottle Apparatus

Student Presenter: Sam Lakenen, Mechanical & Electrical Engineering

Faculty Advisor: Rebecca G. Ong, Chemical Engineering

**Introduction:** A custom, open source roller bottle apparatus was developed that provides a low-cost, easily constructed alternative to existing options on the market. The apparatus is capable of simultaneous mixing of multiple tubes or bottles ranging from 12-61mm in diameter, using a combined rolling and tilting motion. In order to ensure temperature controlled mixing of contents, the apparatus was designed to fit inside a static incubator. In order to increase capacity, up to four tiers of units can be stacked, each with separate speed control.

**Materials and Methods:** Nearly all of the apparatus components were 3D printed or purchased from readily available materials, and the apparatus itself is easily assembled, with minimal hardware requirements. The main body of the device, gears, and minor components were 3D printed and rollers were constructed from PVC pipe. Electronic control of the system was implemented using an Arduino Uno, and a custom printed circuit board was designed and constructed for the device. The apparatus has an LED display with controls for setting the RPM, while tilt angle is fixed by the nature of the design, which is a space-saving feature. Each tier of the apparatus is independently controlled such that different levels can be mixed at different speeds within the incubator.

**Results and Discussion:** With the apparatus still under development we anticipate the completed apparatus to be capable of stacking at least four tiers high and completely contained within the incubator. Development of this completely open-source, easily accessible design for a roller bottle apparatus will allow high schools and universities that can't currently afford a roller apparatus access to conduct cell culture or mixing studies. Additionally, the device can be readily customized to fit the desired application.

## 19. Vertical gradients of leaf and air temperature in a tropical wet forest canopy

Student Presenter: Benjamin D. Miller, Forestry and Applied Ecology  
Faculty Advisor: Dr. Molly A. Cavaleri, School of Forest Resources and Environmental Science

**Introduction:** Tropical forests have evolved under very narrow temperature regimes, and therefore may be more susceptible to global climate change than areas of higher latitude. Upper canopy leaves may already be near or at their thermal maxima, and increasing temperatures could cause permanent damage. Height can impact both the microclimate and physiology of a tropical canopy. Based on previous work, we expected a linear increase in leaf temperature with height and very little air temperature change with height.

**Materials and Methods:** We assessed vertical gradients of air temperature, vapor pressure deficit, leaf temperature, and photosynthetic photon flux density in a Puerto Rican tropical wet forest. We measured within-canopy microclimate using data loggers distributed along a canopy access tower.

**Results and Discussion:** Unexpectedly, leaf temperature was consistent with air temperature at most heights, except for in the upper canopy. Leaf temperature only greatly exceeded air temperature above 17m. The upper canopy was the only location to drastically exceed the known optimal photosynthetic temperature of the measured species by more than a degree. As warming continues, temperatures might continue to exceed the thermal optima of photosynthesis in tropical canopies and potentially cause the tropics to become a weaker carbon sink. This is critical to the global carbon balance as the tropics cycle more carbon than any other biome and the upper canopy cycles a disproportionate amount relative to the remainder of the canopy.

## 20. Puffy Paint: A Novel Material for Microdevice Duplication

Student Presenter: Anna Nelson, Chemical Engineering  
Faculty Advisor: Dr. Adrienne Minerick, Chemical Engineering

**Introduction:** Microdevice fabrication can be an expensive and time consuming process. Current techniques utilize photolithography, which can take approximately 2 weeks and cost ~\$300 to fabricate one silicon wafer. Once a master silicon wafer is created, the features can be replicated with polydimethylsiloxane (PDMS) castings. However, improper processing conditions can cause features to peel off the wafer after being replicated only a few times. The objective of this project was to investigate an alternative method for microfluidic duplication using low-cost, readily available Puffy Paint to extend the life of a silicon wafer and significantly reduce microdevice fabrication time and costs.

**Materials and Methods:** PDMS was cast onto a newly fabricated silicon master wafer. Once cured, a replica mold was created by pressing the feature side of the PDMS into a shallow pool of Puffy Paint. New PDMS was then cast over the cured Puffy Paint. The fabricated devices (master wafer, PDMS castings, Puffy Paint replicas, and PDMS replicas from the Puffy Paint) were compared by measuring the feature's dimensions with a stylus profilometer. Images as well as height ( $\mu\text{m}$ ) and width ( $\mu\text{m}$ ) for each step were compiled to compare the averages and standard deviations.

**Results and Discussion:** This investigation proved that PDMS castings can be replicated using Puffy Paint molds. There were slight variations in size (up to 13%) for each step of the process, which were explained by the processing conditions. The Puffy Paint mold had the largest standard deviations. Feature sizes ranged from 50  $\mu\text{m}$  to 1500  $\mu\text{m}$ ; the largest feature had the most variation in height and the least variation in width, whereas the smallest feature had the least variation in height and the most variation in width. Overall, the general shape and size of the features were not greatly changed by the replication process. This work demonstrated that Puffy Paint can serve as a replication tool and can be used to alter existing features on a silicon wafer, to prototype microdevice designs before investing in costly wafer photolithography, or to teach process steps for designing and fabricating a microdevice.

## 21. Acclimation patterns of stomatal density and size in response to experimental warming and a vertical canopy gradient in four rainforest species

Student Presenter: Elsa Schwartz, Forestry

Faculty Advisor: Molly Cavaleri, School of Forest Resources and Environmental Science

**Introduction:** The tropics are expected to experience unprecedented warming in the near future. Tropical plants have evolved under relatively stable temperatures, so an average increase of 2°C may cause a significant decline in CO<sub>2</sub> uptake if thermal thresholds for photosynthesis are exceeded. By increasing the stomatal density and decreasing the stomatal size, plants can maximize evaporative cooling, which could be beneficial under elevated temperatures. The objective of this study was to measure the effects of both experimental and observational changes in microclimate on stomatal size and density in tropical wet forest understory shrubs and canopy trees. Understory plant stomatal density was expected to increase with a corresponding decrease in stomatal size under experimental warming, and also with increasing canopy height, because a higher density of smaller stomata helps to increase evaporative cooling.

**Materials and Methods:** The tropics are expected to experience unprecedented warming in the near future. Tropical plants have evolved under relatively stable temperatures, so an average increase of 2°C may cause a significant decline in CO<sub>2</sub> uptake if thermal thresholds for photosynthesis are exceeded. By increasing the stomatal density and decreasing the stomatal size, plants can maximize evaporative cooling, which could be beneficial under elevated temperatures. The objective of this study was to measure the effects of both experimental and observational changes in microclimate on stomatal size and density in tropical wet forest understory shrubs and canopy trees. Understory plant stomatal density was expected to increase with a corresponding decrease in stomatal size under experimental warming, and also with increasing canopy height, because a higher density of smaller stomata helps to increase evaporative cooling.

**Results and Discussion:** Contrary to expectations, stomatal size of *P. glabrescens* increased after nine months of warming, but the warming treatment had no effect on stomatal density. For this species, it may be a more cost-effective strategy to have fewer, larger stomata instead of a higher density of smaller stomata under warmer conditions. In support of our hypothesis, stomata of *P. brachiata* decreased in size after nine months of warming. Stomatal density of *P. brachiata*, on the other hand, decreased after three months of warming, but the treatment effect disappeared after nine months of warming. The two species showed opposite responses to experimental warming, revealing two very different strategies. Both stomatal size and density increased with height in the canopy for *P. montana* and *O. sintensis*. This was expected for density, but not for size. It could be that a greater density of larger stomata is more beneficial for evaporative cooling in the hot, dry conditions of the upper canopy.

## 22. Simultaneous Simulation of Mineral Grades using Geostatistical Methods

Student Presenter: Benjamin Sovinski, Geological Engineering  
Faculty Advisor: Snehamoy Chatterjee, Geological and Mining Engineering and Sciences

**Introduction:** Two point statistics is utilized for modelling these two data sets. The issue with this method is it cannot capture the complexity of the shape, structure, grade, and distribution of the ore body and surrounding rock, specifically when it comes to taking into account unknowns within the rock-type and spatial correlation. Since the ore grade model is based off of the lithological model, errors are compounded. Intuitively, further discrepancies occur between the model and real life characteristics of the ore when the data is mapped again to obtain the distribution of ore grades

**Materials and Methods:** This algorithm will be generated and assessed using MatLab. A series of training images will be used to initially test the functionality of the program. A Memo of Understanding between Newmont Mining Corporation (hereafter to be called Newmont) and Michigan Technological University has been signed. Outlined within the memo, is that Newmont will provide us with a data set to be used with the algorithm. Data will be from an already mined out sections of a mine that has recently stopped production.

**Results and Discussion:** What we are proposing to limit these errors is to implement a multiple point statistical method to do the modeling. We will be generating and putting into practice an algorithm that generates a pattern-based simulation using wavelet analysis. This method would take the assay data (data from the drill cores) and use it to simultaneously model both the lithological and the ore grade data. Thus eliminating compounding errors. This method would limit errors to one stage of modelling. This algorithm will use the assay data that Newmont provides and then we will compare it to grade control data (the rock type and ore grades that they actually mined out) to determine its ability to accurately represent the post production data.

## 23. Peptide-Based Nanoparticle for Cancer Therapy

Student Presenter: Deanna Springgay, Biochemistry and Molecular Biology

Faculty Advisor: Martin Thompson, Chemistry

**Introduction:** Researchers have been exploring the applications of gold nanoparticles (AuNPs), for a variety of novel therapeutic uses to fight cancer including drug delivery, photothermal therapy, and cell targeting. Additionally, AuNPs are capable of altering unfavorable pharmacokinetics of drugs. AuNPs can be functionalized with moieties to incorporate additional features, such as controlling drug release, targeting specific cell-types and improving cellular uptake. Peptides are often used as the conjugating moiety as they possess properties ideal for the purpose listed above. In this research, multiple peptide moieties were used to functionalize AuNPs to assess their capacities to serve as drug carrier.

**Materials and Methods:** Gold nanoparticles were created in a reduction of  $\text{HAuCl}_4$  with sodium citrate in water to be around 50nm in diameter. Size was determined using DLS and concentration was determined using Beer's-law. Four peptide/peptide-PEG were designed for functionalization. Each peptide was conjugated to AuNPs via thiol-based exchange reaction by mixing with nanoparticles in excess molarity. As a model of hydrophobic compound, warfarin was used and change in free-drug concentration was monitored by absorbance measurement. The peptide-conjugated nanoparticles were loaded with a hydrophobic drug to examine capabilities to serve as a drug carrier using equilibrium dialysis.

**Results and Discussion:** Multiple conditions were tested for gold nanoparticle preparation and ration of  $\text{HAuCl}_4$  and Sodium citrate has been determined to make 50-nm AuNP. Each of four peptide/peptide-PEG moiety was designed to interact with a hydrophobic drug, thus it is predicted that a decrease in free-drug concentration will be observed by addition of functionalized AuNPs. Currently ongoing testing is to alter the condition (e.g. pH, temperature, and addition of protease) to observe changes in drug release/holding capacities of each functionalized AuNPs. The potential implications of this research are to contribute to the design of AuNPs for drug delivery. For example, a peptide can be designed to contain both targeting and hydrophobic regions to reduce the overall toxicity of a higher dosage, or sequences used for controlled drug delivery may be inserted.



## 24. Phosphorus Levels in Small Local Lakes Phosphorus Levels in Small Local Lakes

Student Presenter: Rachel Stern, Environmental Engineering  
Faculty Advisor: Dr. Noel Urban, Civil & Environmental Engineering

**Introduction:** This research aimed to determine relationships between total phosphorus levels in small lakes in Houghton County and watershed and lake characteristics and chemical composition. Phosphorus levels have been observed to correlate with the methylmercury levels in area lakes, affecting the edible fish population.

**Materials and Methods:** A method to detect low levels of total phosphorus was developed, using the TNT843 Hach kit, the Hach reactor block, and the Hach 1900 or 3900 spectrophotometer. The total phosphorus is converted into orthophosphate with the Hach reagents and reactor block, then dyed blue to be detected by the spectrophotometer. This method is designed for 0.15-4.5 mg/L PO<sub>4</sub>. In order to determine the characteristics of each lake's watershed, ArcMap was used. Lakes were imported from an MDNR polygon file, wetlands from the MDEQ, and a topographical (dem) file from USGS was used. The watersheds were mapped using the GIS software and the important characteristics were recorded. In the field, water samples were collected for phosphorus and absorbance analyses in the lab, a sonde was used to record the temperature, dissolved oxygen, chlorophyll, conductivity, pH, and turbidity at various depths. The data were compiled into an Excel document to determine the correlation between parameters using a two-tail test with 19 degrees of freedom at 95% confidence.

**Results and Discussion:** The correlation analysis revealed significant relationships between phosphorus and secchi depth, absorbance, watershed area, and dissolved oxygen. This is helpful in determining the phosphorus levels in lakes because parameters such as the secchi depth and dissolved oxygen are much easier to measure in the field than the comprehensive total phosphorus methods. Watershed area of a lake can be determined remotely using GIS programs, allowing predictions of phosphorus levels of lakes without travelling to them.

## 25. Preserving the Upper Peninsula Through Soundscapes

Student Presenter: Drew Stockero, Audio Production and Technology

Faculty Advisor: Dr. Christopher Plummer, Visual & Performing Arts

**Introduction:** The goal of my research was to take a look at a potentially indirect way many people have a large effect on the environments considered to be ecologically preserved. While Michigan's Upper Peninsula is largely thought to be well preserved ecological area, noise pollution can potentially have a large impact on an environment. As suggested in work done by soundscape ecologist Bernie Krause, the health of an environment can be determined not just by studying the physical characteristics of an ecosystem, but also by studying the soundscape or the acoustic characteristics.

**Materials and Methods:** To gather the data I went out to various areas of preserved natural significance and recorded in roughly 1 hour periods. Recordings were also gathered at various times of the day for each location in order to account for changes in the soundscape based on time of day. (Typically fauna are more vocal at dawn and dusk) After recordings were gathered they loaded into a sound editing software, Izotope RX, in order to look at their spectrogram. Images of the spectrograms were saved and then annotated with the various sounds seen within them. Particular note was taken to signify which sounds were organically a part of that environment, like animal calls and water, and which sounds were identified as outside interference or noise pollution. The annotated spectrograms were then used in comparison with each other to see the difference between areas featuring noise pollution and areas without.

**Results and Discussion:** The summary of the results gathered would be that noise pollution has a large impact on the ecosystem of a location. Even though all areas where recording took place were physically being preserved the areas that had more consistent noise pollution had distinctly less diversity in the present animal calls. The calls that were present in these affected areas also occupied a much smaller range of frequencies. This shows that the fauna that remain in the affected preserve are only those whose calls are different enough in pitch as to not be muddled by the noise pollution present. The recordings gathered have also been in multiple databases to serve as a current acoustic record of the various locations.

# SURF

## 26. Doctor's Note: A Spatial Analysis of the Built and Social Determinants of Children's Health During the Copper Boom

Student Presenter: Timothy Stone, Civil Engineering

Faculty Advisor: Dr. Don Lafreniere, College of Engineering Social Sciences

**Introduction:** Historical health studies of children provide significant advantages over their contemporary counterparts, specifically with their ability to study at the scale of the individual child. This project utilizes the Copper Country Historical Spatial Data Infrastructure (CCHSDI) to couple 30 years of school attendance and vaccination data to a full recreation of the social (SE) and built environments (BE) of Calumet and Laurium. We examine the role of BE variables such as residential crowding and proximity to industrial activity and SE variables such as family composition and parent's education to uncover who was most susceptible to contracting common communicable diseases.

**Materials and Methods:** The project required acquisition of a multitude of school attendance and health records from the CLK School District. Records were scanned and then transcribed, resulting in a dataset covering a 30-year period and including 29,388 semi-annual records of schoolchildren between 1904 and 1926. This data was then integrated into the CCHSDI through the use of automated and manual geocoding. Geocoding is the process by which textual data, a child's health data in this case, is paired with a location on a map using their address. Using historical geocoders is a new avenue in the realm of historical spatial demographic research, and allowed us to place children with pinpoint accuracy into a 3D model of the actual home they lived in at the time the record was produced. Records which did not fall within the range of the historical geocoder were manually mapped using their contemporary spatialized census records and city directories linked within the CCHSDI. Spatial analysis then linked BE and SE variables to individual children, their siblings, and classmates. A socio-economic (SES) index allowed us to contextualize SE variables such as the parent's education and family situation as well as identifying immigration status and approximate living environment.

**Results and Discussion:** Analysis is ongoing, but initial observations provide a clue for possible findings. Automatic geocoding produces a match-rate of over 80% across most schools, suggesting that the historical geocoding approach is an improvement over traditional methods. Manual review indicates that three primary reasons lead to false positives or no-matches: (1) there were multiple streets with the given name in the town at the time, (2) the child's given address was improperly transcribed, and (3) the map of the given year did not cover the child's location. Initial results suggest that residential crowding and a child's proximity to land used for mining purposes are both expected to have a direct effect on their ability to ward off infectious diseases. Other suspected relationships expected to affect one's susceptibility include the socio-economic status of the child's family, the population density, and the immigration status of the family and child. These findings illustrate the need to look beyond the arbitrary areal unit to individual georeferenced cases to find distinct patterns and trends over time. A SURF application coupled with funding from Dr. Lafreniere will allow me to continue this work into the summer semester.



## 27. Fate of Perfluorinated Compounds in Aqueous-phase Ultraviolet/Persulfate Advanced Oxidation Process

Student Presenter: Rose Turner, Environmental Engineering

Faculty Advisor: Dr. Daisuke Minakata, Civil & Environmental Engineering

**Introduction:** Perfluorinated compounds (PFCs) are an emerging group of contaminants that are potentially carcinogenic to humans and have been found in the drinking water supply. While various water treatment technologies have been evaluated to transfer PFCs between phases (e.g., activated carbon), ultraviolet with persulfate advanced oxidation process (AOP) is an attractive technology because highly reactive sulfate radicals destroy PFCs. However, the removal efficiency and the fate of PFCs in UV/persulfate AOP have not been well understood. In this study, we evaluate the impact of other water quality parameters to the removal of PFCs and the fate of PFCs in UV/persulfate AOP.

**Materials and Methods:** First, the physical chemical properties of PFCs were investigated using the US EPA EPISUITE. Second, electron-density and electrostatic properties of PFCs were calculated using the Gaussian 09 software. Third, the reactivity of sulfate radicals with PFCs and their degradation products were studied by calculating the aqueous-phase free energies of activation and reactions using both the Spartan software and Gaussian 09. Fourth, the removal efficiency of UV/persulfate was determined when PFCs were found in class II surface water. Fifth, a simplified steady-state model and non-steady-state model were developed using the MS Excel spreadsheet and the Fortran compiler, respectively. Sixth, the removal efficiency of PFCs in the presence of various water quality parameters were evaluated using those models. Finally, the model predictions were compared to those that were reported in the literature. As an additional trial, the background dissolved organic matter (DOM) transformation in UV/persulfate batch experiment by using the Orbitrap mass spectrometer to evaluate the impact of DOM to the removal of PFCs was also studied.

**Results and Discussion:** The unique physical chemical properties of PFCs result in their strong carbon-fluorine bond (i.e. solubility of 2290 mg/L at 24°C in water, hydrophilic carboxylate head, hydrophobic fluorocarbon tail). Computational chemistry calculations provided the electron density distribution, which indicate the potential site where electrophilic sulfate radicals attack. The calculated impact of sulfate radicals to the target PFCs in the presence of various water quality parameters revealed that significant amounts of sulfate radicals were scavenged by chloride, iron, and manganese, and little amounts of the radicals are used to destroy the PFCs. This is due to the higher reaction rate constants among these ions. The removal efficacy of PFCs with various operational conditions was evaluated using the simplified steady-state model and non-steady-state model. For example, when the water sample was at a pH of 2, it was shown through the model to have more degraded PFCs than a water sample with a higher pH. In pure water, increasing the hydraulic residence time to 2000 minutes should result in 99% of the PFCs degrading in the plug flow reactor. Finally, batch experiments in UV/persulfate revealed significant transformation of DOM during the removal of PFCs, which implies that other active radical species could contribute to PFC degradation in the presence of DOM.



## 28. Monitoring Migration of Cancer Cells Using a Microfluidic Device

Student Presenter: Brennan Vogl, Biomedical Engineering

Faculty Advisor: Dr. Smitha Rao, Biomedical Engineering

**Introduction:** The survival rate of a cancer patient significantly decreases after a pre-existing tumor begins to metastasize. Metastasis occurs in several steps 1) incursion of tumor cells to local tissue, 2) migration of cancer cells into vasculature, 3) exiting of cancer cells into nearby tissue, circulatory system and lymph nodes and 4) proliferation of cancer cells in new organs. Using microfluidic devices provides a unique approach to monitoring cancer cell migration due to its low cost of production, minimal material use, high sensitivity, and high throughput. By monitoring metastasis in microfluidic devices, a better understanding of the factors influencing cancer cell migration can be found.

**Materials and Methods:** Cancer cell migration is monitored using a microfluidic device fabricated using poly dimethylsiloxane (PDMS). The device forms chambers and channels on a conventional tissue culture plate allowing optical interrogation of adherent cells. In general, for all the studies, cell migration was monitored at 24-hour intervals for a period of 3 days with and without stimulation with cytokines. Image processing (ImageJ) and Matlab were used to perform cell migration analysis on the microfluidic devices. Conventional scratch-wound assay and Boyden Chamber assay were also used to monitor cell migration, as well as, to provide supporting data for the microfluidic experiment. For the Boyden Chamber analysis, a membrane with pore size between 5 $\mu$ m - 8 $\mu$ m, which, was found to be optimal for migration. The number of cells passing across the membrane and the cells remaining on the membrane by MTT assay after harvesting the cells was quantified. Since this is only an end-point analysis, a scratch-wound assay was used. Scratch-wound assay analysis was performed using a confluent tissue culture that was scratched by a p200 pipette tip. The scratched plate was then live imaged using a EVOS FL Auto microscope.

**Results and Discussion:** The aim of this research is to help provide insight into the underlying mechanisms involved in metastasis by studying cell migration. Utilizing Boyden Chamber assays', scratch-wound assays', and microfluidic devices, a comparative analysis of migration between each device will be performed. To provide more data on migration mechanisms, immunostaining will be performed on the microfluidic device and the scratch-wound assay. Additionally, all methods will undergo live-imaging to obtain more data on migration. At this point the research is still ongoing, however, the results so far have shown that cells react to a provided stimulus and traverse the scratch in the scratch-wound assay depending on the amount of stimulus added.



## 29. Aging and the Neurocognitive Mechanisms Underlying Corrective Actions for Obstacle Collision Avoidance

Student Presenter: Allison Waara, Exercise Science

Faculty Advisor: Kevin Trewartha, Kinesiology/Integrative Physiology

**Introduction:** The objective of this research is to identify the mechanisms that allow us to make rapid corrective actions during ongoing movement and to establish how these mechanisms are impacted by aging. Studies have shown that aging is associated with declines in adaptive motor behavior.

**Materials and Methods:** This research investigates the ability to make effective online corrective actions during reaching movements to avoid hitting virtual haptic obstacles by comparing younger adults (n=20) against older adults (n=20). In the obstacle avoidance paradigm, participants reach for virtual targets while grasping a handle and aiming to avoid two parallel obstacles located between the starting position and target. By recording EEG data while participants perform the obstacle avoidance task, we assess whether there are age-related changes in the P3b as a neurophysiological marker of updating and if those changes are what lead to less optimal corrective actions in older adults. In addition to the obstacle avoidance task, we measure individual differences in working memory updating, processing speed, and other executive functions to examine the cognitive mechanisms underlying the ability to make optimal corrective movements.

**Results and Discussion:** A key prediction is that age-related declines in working memory updating explain the proportion of errors in the older adult group, reflecting non-optimal corrective actions. By understanding these mechanisms, we can identify risk factors associated with increases of accidents in older populations.



## 30. Measuring Student Financial Literacy

Student Presenter: Kira Warner, Psychology

Faculty Advisor: Dr. Adam Feltz, College of Sciences and Arts

**Introduction:** As the cost of education and student debt continue to rise, and the financial environment continues to grow more complex, there is an increasing necessity for improved financial decision making. Prior research has focused on financial literacy assessment and education as a way to improve financial decision making across all age groups. Our work involves the following three aims. First, it compares existing measures of financial literacy and how well those instruments predict recommended financial behaviors. Second, we attempt to predict psychological antecedents of financial literacy and recommended financial behaviors. We pay particular attention to the relation of numeracy to financial literacy as it has been shown to be a domain general predictor of good decision making. Finally, we attempt to model student financial literacy with existing financial literacy measures, numeracy, and general demographics. By determining which factors influence financial decision making the most (e.g., numeracy) and understanding the relations among those factors, we can implement more targeted interventions to help students make more informed, better financial decisions.

**Materials and Methods:** Five financial literacy measures and one financial behavior measure were selected for use after a thorough literature review. We also used a 7-item measure of numeracy (i.e., the Berlin Numeracy Test), 10 demographic questions, and the Ten Item personality inventory. Ninety-two participants were recruited using MTU's undergraduate psychology subject pool (through the SONA system), who then received partial credit towards completion of their course research hours. Data was analyzed using JASP (a free user-friendly statistics package) and R Studio.

**Results and Discussion:** Numeracy was consistently correlated with financial literacy measures, more strongly correlated than any of the responses collected from the financial behavior measure. Numeracy was moderately correlated with 4 of the 5 financial literacy instruments ( $r(91) = .27 - .39$ ,  $p < .01$ ) and was weakly correlated with the fifth ( $r(91) = .18$ ,  $p = .1$ ). Numeracy was also a better predictor of financial behaviors than any of the financial literacy instruments. Current work is addressing measurement issues with the financial literacy instruments using Item Response Theory (IRT). We aim to create a better measure of financial literacy. Using this new instrument, we will determine if numeracy is still the dominant predictor of superior financial behaviors when compared to a better financial literacy instrument.

# 31. Electronic Structure Investigations of Sulfenamide Form of Omeprazole in Interaction with the Primary Amino Acid Sites of H<sup>+</sup>/K<sup>+</sup> ATPase

Student Presenter: Travis Wigstrom, Chemical Engineering

Faculty Advisor: Dr Loredana Valenzano, Chemistry

**Introduction:** In an effort to mitigate the symptoms of gastroesophageal reflux disease, proton pump inhibitor (PPI) drugs have been developed to block the production of basal and stimulated acid secretion through the H<sup>+</sup>/K<sup>+</sup> ATPase protein in gastric parietal cells. Among the available PPI drugs, Omeprazole is the most widely used. Omeprazole covalently binds to two amino acid sites (cysteine-813 and cysteine-892) present in the luminal domain of the H<sup>+</sup>/K<sup>+</sup> ATPase protein. This work uses quantum mechanical methods to assess the complexation energies of the sulfenamide species (active form of omeprazole) with respect to its two primary binding sites.

**Materials and Methods:** The investigation was conducted by employing density functional theory (DFT). Atoms were described using a linear combination of atomic orbitals (LCAO) approach as implemented in the Gaussian 09 program, and molecular models were built in GaussView. Geometry relaxation and thermochemical data were determined at PBE/6-311G(d,p) level of theory in vacuum, water, and hydrochloric acid. Single point energy calculations were then performed at 6-311++G(2d,2p) level on the relaxed structures. The two sequences of amino acids surrounding cys-813 and cys-892 were built following a step-by-step procedure where residues were added one at the time around the two cysteine binding sites. The assembly procedure was completed after six amino acid chains were created. Calculations were then performed for all the individual segments with and without the presence of sulphenamide. Complexation energies and corresponding thermochemical data, were determined by applying the Hess' law. A similar procedure was used to determine the complexation energies of the crystalline amino acid structure, with the only difference being the absence of geometric relaxation and frequency calculations for the amino acids as the geometries were extracted from the crystalline structure of the H<sup>+</sup>/K<sup>+</sup> ATPase protein.

**Results and Discussion:** After benchmarking our results against the observed cyclization energy of omeprazole, complexation energies were compared with respect to: (i) The two major cysteine binding sites; (ii) The geometries obtained from a full (gas phase) relaxation and a constrained (crystalline) structure. The influence of the chemical environment was also considered, with all three investigations being done in vacuum, water, and acidic environments. With regards to the cyclization energy of omeprazole, the most noteworthy conclusion is that chemical environment does indeed need to be considered to provide an accurate model. Differences in cyclization energy as large as 52% were observed between the considered chemical environments. A similar trend was seen with the geometrically relaxed complexation energies of the two major binding sites, with both water and acidic chemical environments showing significantly higher complexation energies than the vacuum environment. This observation further supports the need to consider chemical environment when conducting similar investigations. When comparing cys-813 and cys-892 binding sites against each other, no dramatic difference in complexation energy was observed. The same conclusion applies with respect to results obtained according to the two different relaxation approaches.

# SURF

## SESSION B: 3-5 PM

	Presenter	Department	Title
1	Meredith Brehob	Civil and Environmental Engineering Department	Algae and Water Chemistry in Hammell Creek
2	Meghan Campbell	Mathematical Sciences	Risk Premium Analysis for Cyber-Security Insurance in Electrical Grids
3	Virginia Cistaro	Department of Mining and Geological Engineering and Sciences	Comparison of Radial Basis Function (RBF) Approximations to Conventional Numerical Methods for Simulating 3-Dimensional Groundwater Flow
4	Nathan Conner	Department of Chemistry	Ratiometric Near-infrared Fluorescent Probes Based on TBET and $\pi$ -Conjugation Modulation between Tetraphenylethene and Hemicyanine Dyes for Sensitive Detection of pH Changes in Live Cells
5	Owen Cruikshank	Physics	An Exploration of ice nucleation of supercooled water droplets by moving contact lines
6	Hannah Cunningham	Department of Molecular Biology and Genetics	Feasibility of DNA Hairpins as a Nano-thermometer
7	Tania Demonte Gonzalez	Multiphysics Energy Research Laboratory	Development of a Novel Absorption Heat Pump Clothes Dryer
8	Kirsten DePrekel	Geological Engineering	Monitoring the Health of Bridges Using Satellite-Based Persistent Scatterer Interferometry (PSI)
9	Jacob Gould	Computer Science, Discrete Mathematics	Data-driven Exploration of Design Improvements for Probabilistic Text Input
10	Graham Hubbell	Geology Department	Keweenaw Fault Geometry, Secondary Structures, and Slip Kinematics along the Bête Grise Bay Segment
11	Abigail Kanasty	Environmental Engineering Department	Mine Discharges to Creeks of the Keweenaw Peninsula
12	Courtney Kurkie	Kinesiology and Integrative Physiology	Sleep Factors in Collegiate Volleyball Players
13	Alan Labisch	Environmental Engineering	The sources of polychlorinated biphenyl (PCB) compounds in Lake Superior fish
14	Zoë LaLonde	Kinesiology and Integrative Physiology	L-lactate Increases Apoptosis in Dopaminergic-Like PC12 Cells
15	Josh Loiselle	Mechanical Engineering-Engineering Mechanics	"Induced Pluripotent Stem Cell Differentiation to Cardiomyocytes on Conductive Polydimethylsiloxane"

16	Ashley Lingle	Civil and Environmental Engineering	Predicting How Fast Lakes Recover from Mercury Deposition
17	Kaylee Meyers	Biomedical Engineering	Nitric Oxide Releasing Composite Hydrogels for Tendon Repair via Matrix Metalloproteinase Controlled Pathways
18	Madelyn Morley	Kinesiology and Integrative Physiology	Age Differences in the Neurophysiological Correlates of Memory Processes
19	S. Novia Berriel	Physics	Determining Temperature in Air from Raman Scattering Using an Atomic Filter
20	Nicholas Olinger	Mathematics	Evolving Curves with Radial Basis Functions
21	Gemma Oliver	Mathematics	In-Service Teaching Rehearsals: Recognizing and Responding to Teachers' Confidence
22	David Ross	Biomedical Engineering	Bioactive polydimethylsiloxane surface for optimal human mesenchymal stem cell sheet culture
23	Michael Ryan	Social Sciences	Just and Reasonable? Study of Electricity Rates in Houghton County under the Lens of Energy Justice
24	Trevor Simmons	Biomedical Engineering	The Neuroprotective Effect of Human Mesenchymal Stem Cells in a Spinal Cord Ischemia Model
25	Erinn Smith	Chemistry Department	Refining the Purification Process of Histone Proteins
26	Philip Staublin	Alloy Research Central (ARC)	Characterization of Fe-Mn Alloy Phase Diagram in the Low-Temperature Regime
27	David Trine	Biology Department	The Role of Developmental Genes in the evolution of <i>Drosophila</i> Guttifera pigmentation patterns
28	Ayla Vaughn	Kinesiology and Integrative Physiology	Understanding Determinants of Asthma Among Adults in the U.P
29	Derek Verbrigghe	Kinesiology and Integrative Physiology	The Effects of Cognitive Demands and Stress on Prefrontal Cortex Activation and Motor Unit Variability
30	Paige Webb	Biological Science	Understanding Tubercle Microbial Communities and their Impact On Great Lake Structures
31	Luke Weidner	Geological Engineering	Regional Scale Back-Analysis Using TRIGRS: An Approach to Advance Landslide Hazard Modeling and Prediction in Sparse Data Regions
32	Aubrey Woern	Materials Science and Engineering	Distributed Manufacturing of Flexible Products: Technical Feasibility and Economic Viability

# 1. Algae and Water Chemistry in Hammell Creek

Student Presenter: Meredith Brehob, Environmental Engineering  
Faculty Advisor: Noel Urban, Civil and Environmental Engineering Department

**Introduction:** Hammell Creek, near Calumet, flows from the Osceola #4 mine shaft with high metal and metal salts content. Before the stream exits into the Traprock River, it passes through a wetland as well as accumulating runoff, decreasing the metal and salts concentrations. Michigan Tech students have characterized the macroinvertebrate populations at locations along the stream and taken extensive water chemistry measurements for many years. My goal was to build upon past research to observe temporal and spatial trends in water chemistry along Hammell Creek and to compare algal species richness and abundance to that of a reference stream.

**Materials and Methods:** Hammell Creek and Dover Creek were surveyed to identify appropriate sites for sampling, where Dover Creek is the the reference stream with a similar flow and substrate but with different water chemistry. Two algae sampling sites were chosen on each stream: the headwater and a location with rocky substrate. The algal communities of the four sites were assessed by taking three algae samples from each and analyzing them in the lab to identify the family and genus of each alga found. Algal abundance was characterized using rock scrapings. Five samples were taken from each stream at the rocky substrate locations and each sample contained three rock scrapings of a known area. These were dried and then volatilized to find the organic mass. Flow and water chemistry measurements were made or collected from past researchers at the two identified sites on Dover Creek and at seven locations along Hammell Creek.

**Results and Discussion:** There were community differences between the Dover and Hammell sites; the number of genera and families found at the Hammell Creek locations were different from the Dover Creek rocky substrate location to a 90% confidence or greater. There were more types of algae present in the Hammell Creek samples than in the Dover Creek rocky substrate sample. Analysis of algal abundance revealed that there were more algae present in Hammell Creek than Dover Creek. This was also apparent when looking at the streams qualitatively. When conductivity values were grouped by the month in which they were measured, June was different from August at 95% confidence. This probably indicates the lower conductivity in the early summer resulting from increased dilution of salts and metal due to runoff from snow melt. Conductivity values grouped by location showed a significant difference between the mine outflow and the site nearest the exit of the stream into the Traprock River. This indicates the dilution of salt and metal downstream due to accumulation of other waters. Curiously, the expected decrease in conductivity as the stream passed through the wetland was not significant.

## 2. Risk Premium Analysis for Cyber-Security Insurance in Electrical Grids

Student Presenter: Meghan Campbell, Mathematics, Actuarial Science  
Faculty Advisor: Dr. Yeonwoo Rho, Mathematical Sciences

**Introduction:** Increased activity regarding cyber-attacks in the energy sector has brought attention to vulnerabilities within this industry. This was made apparent in December of 2015 when a cyber-attack targeting Ukrainian power companies resulted in a widespread blackout, affecting approximately 225,000 people. Because such an attack could have a cascading effect, we believe an actuarial framework would help mitigate losses for the utility companies and incent them to invest in better technologies by providing policies for different security levels. This project consists of preliminary research into the design of an insurance product which would cover losses incurred by individual power substations in a cyber-attack.

**Materials and Methods:** Because there is little historical data, we chose to perform simulations on the IEEE 30-bus system with the idea that the same method could be applied to a larger interconnection. We simulated changes in profits and calculated the financial loss for individual substations under all possible attack scenarios using Matlab. We categorized the scenarios by the number of nodes under attack and created aggregate loss distributions, weighting each category by likelihood of success. With these aggregate loss distributions, we calculated the mean and variance of the losses for each node, which were used to estimate hypothetical risk premium values using the standard deviation premium principle and the principle of equivalent utility. We also adjusted the distributions for different node protection levels to show the potential benefits utilities could receive by increasing their security levels.

**Results and Discussion:** After initial analysis, we determined it would be most efficient to create separate policies for generation and distribution substations because generation node losses followed a roughly continuous distribution while distribution nodes followed a discrete distribution. We focused on the distribution node policy. Using the standard deviation premium principle, we found that if the node increased security enough to reduce the probability of a successful attack by one half, the risk premium decreases between 30-35%, depending on the node and the risk loading parameter ( $\sim 34\%$  for  $\beta = 0.25$  and  $\sim 32\%$  when  $\beta = 0.5$ ). Further research should describe a policy for generation substations and an aggregate policy, similar to what a utility company owning several substations would purchase.

### 3. Comparison of Radial Basis Function (RBF) Approximations to Conventional Numerical Methods for Simulating 3-Dimensional Groundwater Flow

Student Presenter: Virginia Cistaro, Geological Engineering  
Faculty Advisor: Dr. John S. Gierke, Department of Mining and Geological Engineering and Sciences

**Introduction:** Calculating groundwater flow under realistic conditions requires numerical methods to approximate the solutions to the governing equations. Radial basis functions (RBFs) have long been suited for interpolating spatial data to accommodate abrupt heterogeneities, which are the most challenging and very common in nature. Just recently have mathematicians developed numerical methods to approximate the solutions of differential equations using RBFs. This study presents the results of research done to investigate the effectiveness and efficiencies in using RBFs for solving the groundwater flow equations.

**Materials and Methods:** One common method to model groundwater flow is through MODFLOW. The basis for the model is that it employs the use of Finite Differential Equations (FDEs). The comparison of the two methods, RBFs to FDE, is done through the modeling software application called GMS, which is the modeling environment in which MODFLOW serves as the groundwater flow model (Aquaveo, Provo, Utah). It is one of several standard groundwater flow modeling systems for use by hydrogeological practitioners and researchers, including scientists working for the United States Geological Survey (USGS). This study worked on approximating groundwater flow in heterogeneous conditions using MODFLOW as a suite of benchmark test cases to which to compare the new RBF approach. Benchmark case examples are sets of data paired with known solutions. The benchmark cases analyze which method properly displays the solutions, since the outputs are known. Problems were selected to test the grid-structure because FDEs rely heavily on such a grid. Test cases show the real-world application of the research and the worth of investigating the capacity of the RBF method.

**Results and Discussion:** The 3D modeling results produced examined where both methods fail in accuracy. Specifically, a closer look was given to the behavior of the model on grid lines and around groundwater well singularities, since FDEs struggle to represent these parts of the model accurately. This research looked at the influence of spatially variable aquifer properties, such as hydraulic conductivity. Care will be taken to investigate the smoothness of the model and how accurate it is on the grid lines and the space around a well and compare to see if RBFs render that space more accurately and efficiently. If the RBFs prove useful, then the grid-structure and its inadequacies can be removed. Testing MODFLOW with RBF approximations helped determine if RBFs are more accurate and robust than using FDE for flow and transport problems.

## 4. Ratiometric Near-infrared Fluorescent Probes Based on TBET and $\pi$ -Conjugation Modulation between Tetraphenylethene and Hemicyanine Dyes for Sensitive Detection of pH Changes in Live Cells

Student Presenter: Nathan Conner, Biochemistry and Molecular Biology  
Faculty Advisor: Dr. Haiying Liu, Chemistry

**Introduction:** In the past, fluorescent dyes have been developed using Rhodamine based on FRET strategies and showed emissions in the 600 nm range. In this paper development of three probes with emissions in the near infrared range using TBET and  $\pi$ -conjugation modulation strategies are outlined. These probes use Tetraphenylethene and Hemicyanine dyes as donor and receiver respectively in TBET. These probes are important in the detection of intracellular pH to limit photodamage while still maintaining selective and ratiometric measures of pH in a biological sample.

**Materials and Methods:** In the past, fluorescent dyes have been developed using Rhodamine based on FRET strategies and showed emissions in the 600 nm range. In this paper development of three probes with emissions in the near infrared range using TBET and  $\pi$ -conjugation modulation strategies are outlined. These probes use Tetraphenylethene and Hemicyanine dyes as donor and receiver respectively in TBET. These probes are important in the detection of intracellular pH to limit photodamage while still maintaining selective and ratiometric measures of pH in a biological sample.

**Results and Discussion:** Three near-infrared fluorescent probes were developed using the TBET and  $\pi$ -conjugation modulation strategies. These probes all display strong TPE fluorescence at neutral and basic pH, and overcome imaging blind spots typical of other fluorescent pH probes. On top of this, the probes show little cytotoxicity, are very photostable, high membrane permeability, as well as a sensitive and selective response to pH over metals, anions, and amino acids. Specifically, Probe A shows AIE properties while B and C lack them. All three display ratiometric response to changes in pH in cellular environments ranging from pH 7.0 to 3.0. Probe A specifically displays high sensitivity to pH changes when compared to B and C with very high signal to background ratios. These results allow for future development of ratiometric probes that allow for detection of a variety of other molecules including metal ions, reactive oxygen and nitrogen molecules, and thiols. This would be done by introduction of new ligands that are sensitive to these species to the hemicyanine.

## 5. An Exploration of ice nucleation of supercooled water droplets by moving contact lines

Student Presenter: Owen Cruikshank, Physics  
Faculty Advisor: Dr. Raymond Shaw, Physics

**Introduction:** Supercooled water, liquid water below 0 degrees Celsius, exists in an unstable state and makes up many clouds. Supercooled water only freezes or nucleates if the water becomes extremely cold (around -40 degrees Celsius) or if it is in contact with another material (around -25 degrees Celsius on glass). Previous work has shown that a moving contact line (the interface between the water droplet, surface, and air) can cause a supercooled water droplet to freeze spontaneously at a higher temperature than usual. The goal of this research is to determine the role of the moving contact line in ice nucleation.

**Materials and Methods:** A temperature and humidity controlled chamber was used for the experiments. A high-speed camera running at 5000 fps was used to view how the water droplets froze. It was hypothesized that inward droplet curvature of the moving droplets caused negative pressure within the droplet and helped the water droplets freeze. To study this, a droplet was held between two planes of glass and pulled apart to create inward curvature by tension. Alternating stripes of hydrophobic and hydrophilic surfaces 1mm apart were also used to create inward curvature and distorted contact line. Previous work used a vertically oscillating surface to create contact line movement. A new apparatus was built to move the droplet horizontally to view the droplet movement more clearly. The new apparatus uses a solenoid to move the surface underneath the droplet. Trace amounts of oil caused a distorted contact line in previous work. The water is tested pure and with trace amounts of oil.

**Results and Discussion:** The experiments to create inverse curvature failed to increase the freezing temperature of the supercooled water droplets. It was hypothesized that a negative pressure of  $10^8$  Pascals would be required to create a 10-degree Celsius increase in freezing temperature. To create a negative pressure that great would require separation on the scale of microns. The facilities to create surfaces on that scale were not feasible within the time span of the project. The apparatus to move droplets horizontally is working successfully. Supercooled water with a small amount of oil has frozen with actuation from the solenoid but pure water has not. These experiments are ongoing and more data must be collected to make conclusions. Possible causes of freezing are: droplet pinning or sticking to the surface, water and oil mixing creating small oil droplets and large pressure changes, or cavitation.

# SURF

## 6. Feasibility of DNA Hairpins as a Nano-thermometer

Student Presenter: Hannah Cunningham, Biomedical Engineering  
Faculty Advisor: Caryn Heldt, Molecular Biology and Genetics

**Introduction:** As demand for miniaturized devices increases, there is a demand for nano thermometers to evaluate performance intracellularly and in vitro. A novel method to create nano thermometers is with DNA hairpins. DNA hairpins are oligonucleotides with complementary ends that bind together, creating a hairpin structure. The hairpins were tagged with a fluorophore that can indicate a change in the structure induced by temperature. This change in structure is called melting. Having a linear response for a specific temperature range, these probes can have a tailored DNA sequence for a target temperature range.

**Materials and Methods:** DNA sequences are composed of A–T and G–C bonds. The melting temperature of these bonds are different. Hairpins with a varying number of G–C bonds were tested to determine the effect of the number of G–C bonds in the hairpin had on the melting temperature. Each hairpin was tested in three different solutions, distilled water mixture, 200 mM Tris-HCl of pH 8, and 200 mM NaCl. Samples were loaded into a thermocycler and were cycled through a program that cycled the temperature from 70°C to 25°C 9 times. After determining there was a lack of similarity during the 9 cycles, the experiment was repeated again with eight quick cycles from 95°C to 25°C followed by the 9 cycles of 70 degrees to 25 degrees to determine the effect it had on hairpin opening.

**Results and Discussion:** The hairpin performance when cycling from 75°C to 25°C was poor. The response was not constant between cycles, making the hairpin an unreliable sensor. By adding eight successive jumps between 95°C and 25°C prior to measurement of the hairpin response with cycles from 70°C to 25°C, the response became more consistent. This could be due to the increase mechanical movement of the hairpin as it switches from the open form at 95°C and the closed form at 25°C. This data suggests that before using a hairpin, the hairpin should experience a change in temperature in quick succession to reach stability.

## 7. Development of a Novel Absorption Heat Pump Clothes Dryer

Student Presenter: Tania Demonte Gonzalez, Mechanical Engineering  
Faculty Advisor: Dr. Sajjad Bigham, Mechanical Engineering- Engineering Mechanics

**Introduction:** By being in 80% of households in the US, clothes dryers have become one of the major home appliances in the country. Currently, there are two types of clothes dryers: vented and ventless clothes dryers. Both types of clothes dryers have improved their features over the years, making them up to 20% more efficient over the past five years. However, even though they are more efficient than in the past, there are still not efficient enough to today's standards.

**Materials and Methods:** In this study, we introduce a novel Absorption Heat Pump Clothes Dryers (AHP-CD), which was modeled using the software EES, based on mass equilibrium equations and energy equilibrium equations, demonstrating at least 100% more efficiency than current CD technologies. In the heart of the proposed technology, there is a closed absorber module. The humidity of the air existing from the clothes dryer drum is reduced in the evaporator module due to the accompanying condensation process. The less humid air is then sent to the absorber module to gain heat generated in the absorption process. The warm air is then directed to the condenser module to get hot before sending back to the drum. The absorption model, does not only take advantage of the latent heat of the water present on the hot air, but it also absorbs most of the moisture coming from the wet clothes, allowing the wet clothes to dry faster with less energy consumption. This new method of heating air notably reduces the consumption of electricity when compared to existing electric heated clothes dryers. The absorption system consumes mainly natural gas, which makes this clothes dryer more efficient and environmentally friendly.

**Results and Discussion:** The results derived from EES showed that the Primary Coefficient of Performance (PCOP) of the Absorption Heat Pump Clothes Dryer can vary depending on the initial temperature and relative humidity of the clothes, as well as the air velocity inside the drum. When compared to the current most efficient clothes dryers in the market, the novel AHP-CD on an electric basis can be 10 times more efficient, and on a gas basis, the AHP-CD could be 3 times more efficient. In summary, even though there is still more to research about this new model, the innovative Absorption Heat Pump Clothes Dryer could be the most efficient and environmentally friendly alternative to current clothes dryers.

## 8. Monitoring the Health of Bridges Using Satellite-Based Persistent Scatterer Interferometry (PSI)

Student Presenter: Kirsten DePrekel, Geological Engineering  
Faculty Advisor: Thomas Oommen, Geological Engineering

**Introduction:** Transportation is a critical element for the advancement of society. Bridges are vital for an efficient transportation network. Bridges across the world undergo variable deformation due to Earth's dynamic processes. This displacement is caused by ground motion which occurs from a number of natural and anthropogenic events. Deformation causing events include weather/temperature variation, subsidence, landslides, earthquakes, water/sea level variation, oil pumping, undercut slopes, mining, etc. Continually displacement and deformation may cause bridge failure, putting civilians at risk if not managed properly. Monitoring the displacement of bridges, large and small, provides evidence of the state and health of the bridge.

**Materials and Methods:** Traditionally, monitoring of bridges has been executed through on-site visits and other various site-based instrumentation. Although this method of bridge monitoring is systematic and successful, it is not the most efficient and cost effective. Through technological advances, satellite-based Persistent Scatterer Interferometry (PSI) and Geographic Information Systems (GIS) have provided a system for analyzing the velocity at which ground deformation occurs over time. This method is applied to distinguish the bridges that are more at risk than others through generating models which display the displacement at different locations along each bridge. A bridge's health and its potential risk can be estimated upon analysis of measured displacement rates. In return, this process of monitoring bridges can be done at much faster rates; saving time, money and resources.

**Results and Discussion:** PSI data covering Oxnard, California and Palos Verdes Hills, revealed both bridge displacement and large-scale ground displacement. Ground displacement patterns surrounding each bridge provided reason for the type of displacement occurring for each bridge. With this analyzation process it was determined that bridges within the Oxnard area displayed larger velocity of displacement than those near Palos Verdes Hills. Although each bridge maintained different patterns of displacement, the majority of bridges within the Oxnard area displayed an overall downward movement matching regional subsidence trends observed in the area. Patterns in displacement-time series plots provide evidence for two types of deformation mechanisms. Long-term downward movements correlate with the relatively large regional subsidence observed in Oxnard and east of the Palos Verdes Hills. Thermal dilation from seasonal temperature changes may cause short-term variabilities unique to each bridge. Overall, it may be said that linking geologic, weather and groundwater patterns with PSI data has been proven to be a successful method for monitoring bridges.

## 9. Data-driven Exploration of Design Improvements for Probabilistic Text Input

Student Presenter: Jacob Gould, Computer Science  
Faculty Advisor: Dr. Keith Vertanen, Computer Science

**Introduction:** Text input is a common way people communicate with each other and with machines. Often text input relies on a probabilistic auto-correction algorithm. In past work, we have used a decoder named VelociTap to infer users' intended text from noisy tap input on phones and watches. In past experiments, we have logged numerous examples of users' input including aspects not used in our recognition algorithm such as the timing of taps. This research explores using different machine learning algorithms to learn patterns from these other aspects of the input data to try and predict if a given input is likely to be recognized incorrectly.

**Materials and Methods:** We used data collected from past user studies which consisted of what the user meant to type, and a sequence of tap data containing tap locations and times. We processed the raw input data using VelociTap to obtain the recognition result for each input. We enriched the input observations with metadata including whether the decode was correct, the average time between taps, the maximum distance between taps, and the number of taps. We split the data using 80% as a training set and 20% as a test set. We trained a range of models including support vector machines, linear regression, and K-means clustering. We tested the trained models, producing an error rate matrix. We separately analyzed data collected on a smartwatch and on a smartphone.

**Results and Discussion:** We found our best models were able to predict recognition errors less than 10% of the time. Thus it appears there is not a strong correlation between features in the metadata and whether the input was correctly recognized or not. These results could mean we have not yet collected enough data to train a robust model, that the learning model hyperparameters need further optimization, or that we need to search for other features that may be more predictive of likely recognition errors.

## 10. Keweenaw Fault Geometry, Secondary Structures, and Slip Kinematics along the Bête Grise Bay Segment

Student Presenter: Graham Hubbell, Geological Engineering  
Faculty Advisor: James DeGraff, Geological Engineering

**Introduction:** The Keweenaw fault is a major reverse fault that generally strikes northeast along the Keweenaw peninsula and dips northwest at angles between 20° and 85°. East of Lac La Belle at its northern reaches, the fault changes strike to an east-southeast direction. The fault was previously mapped along Bête Grise Bay in the 1950s by the USGS, however contradictions in its geologic interpretation have arisen over the years. Our research focuses on the geometry of the Keweenaw Fault, nearby related faults, and their slip motion along the Bête Grise Bay shoreline, and includes both onshore and offshore mapping.

**Materials and Methods:** Our field work has involved making geologic observations of rock type, measuring structural orientation, and collecting positional data with 1-meter precision using Trimble DGPS units. We also collected rock samples at significant outcrops for later microscopic work and lab analyses. During field work we kept notes and identified areas for more detailed future observations. We used a Geometrics magnetometer to measure the Earth's magnetic field intensity along survey lines. The idea behind this method is that the Jacobsville Sandstone south of the fault would have a lower, more subdued magnetic field relative to basalt north of the fault, which has greater quantities of magnetic minerals. We set up a grid of lines in areas straddling the fault contact in order to map its location. During more detailed geological observations, we used a Brunton compass to measure strike and dip of the major rock layers and structures. In the lab, we have plotted the magnetic data and the high-precision GPS locations in ArcGIS, which will be used to produce our final maps.

**Results and Discussion:** While the work is ongoing, our research shows that the newly mapped fault trace does not agree with previous mapping and interpretation. Previous geologists interpreted any contact between Portage Lake Volcanics (basalt) and Jacobsville Sandstone as a fault. At several locations we have observed a stratigraphic contact between these two units, whereby younger sandstone lies atop older basalts with no sign of faulting between them. Our work also reveals an en echelon system of fault segments rather than the geologically unusual, sinusoidal, fault trace mapped in the 1950s. As its orientation changes to an easterly trend, the fault splays into multiple fault segments with east-southeast orientation. Our research also shows that PLV layers along the shoreline dip steeply to the southeast, whereas the relevant USGS map shows the layers dipping northward. These new observations may indicate the presence of a large fold north of the Keweenaw fault because PLV layers a few miles north of the shoreline do in fact dip northward. This work has improved the location accuracy of geologic structures relative to previous maps because we are using a high-precision GPS, which technology did not exist at the time of previous mapping.

# 11. Mine Discharges to Creeks of the Keweenaw Peninsula

Student Presenter: Abigail Kanasty, Environmental Engineering  
Faculty Advisor: Noel Urban, Civil & Environmental Engineering

**Introduction:** Fish throughout Michigan's Upper Peninsula (UP) have high mercury contamination levels; some of this may result from historical mining. Back when the Keweenaw mines were active, they were deliberately dewatered. Now that they are closed, they fill up due to seepage of rainwater, and this water can be discharged into local creeks. It is possible that the high mercury in Keweenaw fish relates to mine discharges. Mercury is a health hazard to both humans and ecosystems. It can cause neurological, cardiovascular and immunological problems. The goal of this project was to identify active mine discharges into surface waters.

**Materials and Methods:** The first step was to determine the locations of mines and possible discharge sites. To get a general location, online sources, the MTU archives and tips from professors and other credible personnel were used. Google Earth was used to get an overview of the area before visiting the location. Coordinates were recorded from Google Earth, and a GPS was used to find the location in the field. The surrounding area was searched for mine shafts and adits, ruins, nearby creeks and direct mine discharges. Probes were used to measure water for abnormally high values of conductivity and low values of pH. Creeks with a conductivity over 200  $\mu\text{S}/\text{cm}$  were investigated further for mine discharge by hiking upstream to find the source. An Excel spreadsheet was used to compile the field data. ArcMap was then used to map the mine locations as well as the conductivity for each location visited. Conductivity layers were created using other acquired data as well. The conductivity layers were superimposed on maps of mine shafts and tunnels to associate mine discharges with former mines. A literature search on mine discharge remediation was performed to identify options for cleaning up the ongoing sites of contamination.

**Results and Discussion:** Three main mine discharges were located. The first location, Owl Creek, was part of the Copper Falls Mine. Although conductivity did not exceed 200  $\mu\text{S}/\text{cm}$ , the values stood out compared to the conductivity of creeks in the surrounding area. The second location was from Quincy Mine. A creek running along the tram tracks near the tourist adit, was found to have very high conductivity. It is thought that the old dewatering system that drained out of the nearby adit and flows into the old Quincy reservoir may still be operative. The third location had the highest conductivity of all the measured locations. This is the location of the Osceola number four shaft, just outside of Calumet. It is believed from local lore that the mine shafts from Mohawk to Osceola are interconnected and discharge at this location. Since this is an environmental issue, remediation methods are being assessed for feasibility. Possible methods include permeable reactive barriers, sulphur polymer stabilization/solidification (SPSS), precipitation/coprecipitation, and stabilization/solidification with sulphur microcements. Remediating mine discharge is a step in the right direction for the removal of mercury contaminants.

## 12. Sleep Factors in Collegiate Volleyball Players

Student Presenter: Courtney Kurkie, Exercise Science  
Faculty Advisor: Jason Carter, Kinesiology/Integrative Physiology

**Introduction:** Sleep deprivation has been shown to have a negative effect on cognitive and physical performance, thus the purpose of this study was to compare objective sleep patterns during home week vs. away (i.e., travel) week of in-season, collegiate Division II volleyball. Objective sleep measures included total sleep time, sleep onset latency, sleep efficiency, wake after sleep onset (WASO), and number of awakenings. We hypothesized higher sleep quality during home game series compared to an away game series.

**Materials and Methods:** Fourteen collegiate women volleyball players (age range 18-21 years) were tested for five consecutive weekdays twice - once during a home week series and once during an away week series. During each week, there were back-to-back games on Thursday and Friday. Objective sleep was determined back upon wrist actigraphy, while subjects sleep was determined using daily sleep diary. Prior to beginning actigraphy recordings, heart rate and blood pressure were determined to ensure subjects were in a normal range. Data from Monday, Tuesday, and Wednesday were averaged to represent a "baseline" sleep, while Thursday and Friday were averaged to represent "game night" sleep. Paired t-tests were used to compare objective sleep across the two weeks, and  $p < 0.05$  (two-tailed) was considered significant.

**Results and Discussion:** Total sleep time during baseline was significantly lower during the away week compared to the home week ( $6.4 \pm 1.8$  vs.  $7.2 \pm 1.9$  hours;  $p = 0.001$ ), but was not different on the game nights ( $6.8 \pm 1.8$  vs.  $6.7 \pm 3.7$  hours;  $p = 0.583$ ). Consistent with total sleep time data, the number of nocturnal awakenings during the baseline was higher during away week ( $36 \pm 27$  vs.  $28 \pm 16$  awakenings;  $p = 0.001$ ), but was not different on the home vs. away game nights ( $30 \pm 26$  vs.  $28 \pm 17.6$  hours;  $p = 0.400$ ). Sleep efficiency, sleep onset latency, and WASO were not different across home and away weeks during baseline or game nights. In summary, home and away series showed differences in total sleep time and number of awakenings, suggesting adjustments should be made to allow more sleep prior to away travel games.



# 13. The sources of polychlorinated biphenyl (PCB) compounds in Lake Superior fish

Student Presenter: Alan Labisch, Environmental Engineering  
Faculty Advisor: Judith Perlinger, Civil & Environmental Engineering

**Introduction:** Polychlorinated biphenyl (PCB) compounds are a category of 209 toxic environmental contaminants. They were used in industrial processes until the 1970s and are of concern due to their persistence in the environment and their harmful effects on animals. PCBs enter water bodies through the air, and are especially prominent in the Great Lakes region due to each lake's large surface area. Understanding PCB sources to Lake Superior fish is important to determine how to reduce their concentrations most effectively. We hope to assist policy makers in designing policies that decrease PCB inputs quickly without further affecting biota.

**Materials and Methods:** The seven most-studied PCBs were analyzed by looking at gaseous concentrations over the past 15 years. Days with extremely high or low concentrations were analyzed with NOAA's Hybrid Single Particle Lagrangian Integrated Trajectory (HYSPLIT) model software to generate trajectories showing where those air parcels traveled before reaching the monitoring site.

Gaseous PCB concentrations were retrieved from a monitoring site in Eagle Harbor, MI. As part of the Great Lakes Integrated Atmospheric Deposition Network (IADN), this station is used to monitor the temporal trends of atmospheric contaminants. Using an enthalpy analysis technique similar to Subhash and Honrath (1999), past days with unusually high or low PCB concentrations were determined and used as inputs into HYSPLIT.

HYSPLIT models air as it moves around the globe. Keweenaw air-mass transport patterns on the specific days detected in the data analysis were examined with HYSPLIT, generating back-trajectories for each tested PCB compound. The trajectories were used in Geographic Information Systems (GIS) software to create maps of each air mass trajectory so the origins of the PCBs could be determined. In the future, the trajectory results will be analyzed using Positive Matrix Factorization (PMF) to determine if different transport pathways are associated with different PCB mixtures.

**Results and Discussion:** Plots of log concentration versus inverse absolute temperature were generated for each PCB congener. The analysis showed a number of days with 'extremely high' or 'extremely low' concentrations, defined as more than two standard deviations away from the mean concentration value. These dates were used in the trajectory analysis.

Trajectory analysis of the 42 total 'extremely high' and 'extremely low' concentration dates occurring between 1991 and 2011, resulted in trajectories that originated mostly in the northwestern quadrant. To interpret these results further, PMF must be conducted.

## 14. L-lactate Increases Apoptosis in Dopaminergic-Like PC12 Cells

Student Presenter: Zoë LaLonde, Biochemistry and Molecular Biology  
Faculty Advisor: Qing-Hui Chen, Kinesiology and Integrative Physiology

**Introduction:** Lactate has been shown to be excitatory through activation of ligand gated calcium channels. Studies have demonstrated that extracellular lactate is capable of activating N-methyl-D-aspartate receptors (NMDAR), acidifying neurons and glial cells, which may contribute to excitotoxicity. Since cerebrospinal fluid (CSF) lactate concentrations are elevated in several neurodegenerative disorders, including Parkinson's disease, we tested the hypothesis that increased L-lactate may be a contributing factor to excitotoxicity of dopaminergic like PC12 cells.

**Materials and Methods:** Nerve growth factor derived PC12 cells were exposed to increasing concentrations of L-lactate (0mM, 1.5mM, 2mM, 3mM, 4mM and 8mM) for 4 hrs which increased cell death in a dose dependent manner, analyzed via flow cytometry using propidium iodide (PI) exclusion. The (EC) 50 value was found to be 3.30 mM. The percent of cells staining positive for PI were significantly increased ( $P < 0.05$ ): control, 0 mM L-lactate, 15.0 +/- 0.5 % (n=4) and 4 mM L-lactate, 31.6 +/- 4.6% (n=4).

**Results and Discussion:** This data suggests that elevated CSF lactate may be a contributing factor to dopaminergic cell death in Parkinson's disease.



## 15. “Induced Pluripotent Stem Cell Differentiation to Cardiomyocytes on Conductive Polydimethylsiloxane”

Student Presenter: Josh Loiselle, Mechanical Engineering

Faculty Advisor: Dr. Parisa Abadi, Mechanical Engineering-Engineering Mechanics

**Introduction:** Myocardial infarction is one of the leading killers in both men and women, making the need for new treatment methods even greater. Using cardiomyocytes (CM) differentiated from induced pluripotent stem cells (iPSCs) could allow patients to have a better quality of life and increase the survival rate of myocardial infarctions. Previous studies have shown that carbon-based conductive substrates can enhance cell-cell communication resulting in enhanced iPSC differentiation to mature CM. We propose the use of soft, cross-linkable PDMS with conductive nano-fillers to tailor mechanical and conductive material properties simultaneously.

**Materials and Methods:** Conductive PDMS is made up of PDMS, a silicon based polymer, and a conductive filler, often metal nanoparticles or carbon nanotubes (CNT). This material has the potential to change cell behavior due to differences in conductivity, surface type and stiffness. PDMS will be created using a base kit of elastomer and curing agent, and then mixing in the conductive filler. In this experiment, silver nanoparticles (SNP) and multi-walled CNT (MWCNT) will be tested. The iPSCs will then be cultured on the conductive PDMS and the cells will be differentiated into CM (iCM). In addition, the mechanical and electrical properties of the material will be determined to see if different properties affect the cell behavior. The goal of this research is to increase the maturity of the iCM and determine if further research of conductive PDMS would be beneficial.

**Results and Discussion:** Both harder cured (65° C cross-linking) and softer uncured (room temperature cross-linking) samples for each filler and control PDMS were tested. Cured SNP-PDMS enhanced differentiation of iPSCs to iCM based on the enhanced expression of early cardiac mesoderm marker Homeobox protein NKX-2.5 as well as CM marker Troponin T (TNNT2) relative to control PDMS and glass coverslip, as assessed by immunofluorescence studies. Uncured SNP-PDMS as well as both normal (cured and uncured) PDMS showed reduced gene expression signals. However, uncured normal PDMS had enhanced expression relative to normal PDMS demonstrating a complex relationship between material stiffness and conductivity. Differentiation experiments using MWCNT-PDMS with ~100 times lower filler mass (due to high aspect ratio of CNT) are ongoing.



## 16. Predicting How Fast Lakes Recover from Mercury Deposition

Student Presenter: Ashley Lingle, Environmental Engineering  
Faculty Advisor: Noel Urban, Civil and Environmental Engineering

**Introduction:** Once mercury is deposited into lakes from the atmosphere, it can build up in fish, which then can cause humans to be exposed to this pollutant and suffer health issues. Knowing how fast lakes recover from this pollution can help regulators know how quickly and how much mercury deposition must be decreased. The objective of this research was to use a recently developed model to estimate the magnitude of response expected from different categories of lakes in Michigan's Upper Peninsula (UP) to reductions in mercury deposition due to current regulations.

**Materials and Methods:** This project started with the collection of water quality data from online databases for lakes in the UP. After the data was collected and a quality check of the data was completed, a new database was created using Microsoft Access to facilitate retrieving subsets of the data. Separately, a literature review was performed to determine the lake and watershed characteristics that affect mercury concentrations in lakes. The lakes in the local database were then categorized into groups based on the important parameters identified in the literature search and the statistical distributions of those parameters in the UP lakes. Using a recently-developed model for mercury cycling in a single lake, I next assigned mercury process rates to each category of lakes based on my review of the literature. The model was run for a prototype lake in each category to predict the change in mercury concentration that would result from different scenarios of mercury deposition. Model predictions were compared with mercury concentrations available for these lake categories. Ultimately, these results will be extrapolated to all lakes in the UP based on the relative abundance of each lake category.

**Results and Discussion:** Water quality and watershed characteristics were collected for 250 lakes in the UP. Mapping in GIS revealed few geographic patterns in the lake characteristics important for mercury cycling. Based on the literature review, the following lake and watershed characteristics were identified as important for mercury cycling: watershed size, lake depth, amount of wetlands in watershed, chlorophyll concentration, DOC concentration, and pH. These characteristics resulted in 12 categories of lakes; appropriate process rates for mercury methylation, demethylation and photodemethylation were assigned to each category. The model was applied to lakes with mercury measurements for three of these categories; agreement of modeled and measured mercury will be presented for all three lakes. Application of the model to the remaining lake categories and extrapolation to all UP lakes is still in progress.

# 17. Nitric Oxide Releasing Composite Hydrogels for Tendon Repair via Matrix Metalloproteinase Controlled Pathways

Student Presenter: Kaylee Meyers, Biomedical Engineering  
Faculty Advisor: Rupak Rajachar, Biomedical Engineering

**Introduction:** Tendinopathy is typically the result of excessive overloading, which can affect normal tendon architecture and tenocyte morphology through the degradation of the extracellular matrix (ECM). Currently, acute and chronic tendinopathy injuries are treated with moderately effective reconstructive surgeries and anti-inflammatory steroids. Minimally invasive injectable hydrogels composed of polyethylene glycol (PEG)-fibrinogen that have the ability to release nitric oxide (NO) provide an alternative approach to accelerating wound repair in tendon related injuries. The aim of this work is to assess the activation of ECM-degrading enzymes known as matrix metalloproteinases (MMPs) in the presence of our NO releasing hydrogels.

**Materials and Methods:** Control PEG-fibrinogen hydrogels and NO releasing SNAP-fibrin hydrogels were prepared as per a previously established protocol by our lab. To evaluate cell viability on the hydrogels, live/dead fluorescence imaging and MTT assays were conducted. Tenocyte proliferation and morphology was assessed with established DAPI and Phalloidin fluorescent staining protocols. A standard gelatin zymography protocol was used to assess the activity of MMP-2 and MMP-9 in the media surrounding primary tenocytes on hydrogels at three time points (24h, 48h, 72h). All media samples were normalized by protein content using a BCA assay. Following electrophoresis on 0.1% gelatin / 7.5% acrylamide gels, SDS was removed with a Triton X100 solution and developed overnight at 37°C. Gels were stained with Coomassie brilliant blue and destained to visualize white bands of proteolytic activity against a blue background. MMP activity was quantified with scanning by measuring band intensity and normalized to active MMP standards.

**Results and Discussion:** In this work, we have synthesized a biocompatible, injectable hydrogel composite that serves as a provisional matrix and delivery vehicle for NO. Initial biocompatibility studies confirm that the hydrogels are non-cytotoxic. One of the physiologically relevant effects of NO is the activation and inhibition of MMPs, and when triggered by inflammation, MMPs degrade network collagens and extracellular matrix (ECM) proteins. The regulation of MMPs by their inhibitors (TIMPs) is required to maintain ECM homeostasis and failure to breakdown damaged ECM can lead to tendinopathy. In addition, the early activation of MMPs generally ameliorate the wound healing process. Preliminary experiments suggest NO releasing SNAP-fibrin hydrogels significantly activate MMP-9 in tenocyte culture compared to control hydrogels. Further studies are being conducted to evaluate MMP activation in response to varying NO flux. Future experiments related to this work include developing a tendon-specific cell culture model to determine if mechanical properties, such as varying substrate stiffness, effect the activation of MMPs. The results of these experiments will be used to regulate the release of MMPs with our NO releasing fibrin hydrogels to promote stable wound healing.

## 18. Age Differences in the Neurophysiological Correlates of Memory Processes

Student Presenter: Madelyn Morley, Exercise Science  
Faculty Advisor: Kevin Trewartha, Kinesiology and Integrative Physiology

**Introduction:** The proposed research will examine age differences in the neurophysiological correlates of memory processes involved in motor learning in healthy aging. An important cognitive process that may contribute to motor learning is the ability to update working memory (WM) with task relevant information. Electroencephalography (EEG) studies with an event-related potential (ERP) design have identified a neurophysiological correlate of WM updating called the P3b component. We will test the hypothesis that reductions in the P3b are related to age-related changes in the ability to adapt motor responses to changing task demands in the early stages of motor learning.

**Materials and Methods:** For this project the motor learning tasks were implemented using a robotic device called a KINARM (B-kin Technologies) housed in Dr. Trewartha's laboratory. During the motor learning task we also collected continuous EEG data using a 32-channel active electrode Active Two system (BioSemi). In addition to the motor task, we asked participants to perform a battery of cognitive tests (including the Stroop task, Flanker task, N-back task, and Paired-associate learning task) to assess overall cognitive status of our participants. The cognitive task battery is implemented using PEBL (The Psychology Experiment Building Language) software. We are aiming for a final sample of 20 younger adults (18-35 years old) and 20 older adults (60-85 years old), with equal numbers of males and females in each age group. For this research we compare the performance of younger to older adults, and assess bivariate correlations between the cognitive measures and motor learning in both age groups. We are testing two main hypotheses: 1) that aging is associated with declines in early learning due to alterations in the fast process for motor learning, and 2) that those early learning deficits are the result of diminished WM updating processes, as reflected in the P3b ERP component.

**Results and Discussion:** The research is currently ongoing. This research will establish the utility of the explicit aim reporting method for identifying age-related changes in the implicit and explicit memory contributions to motor learning, and determine the neurophysiological correlates of early stages of motor learning. Ultimately, these findings will motivate future studies on the impact of Alzheimer's disease on motor performance, and will inform the design of a more portable version of a motor learning task that can be readily administered in a clinical setting to contribute to the diagnosis of Alzheimer's disease.

## 19. Determining Temperature in Air from Raman Scattering Using an Atomic Filter

Student Presenter: S. Novia Berriel, Applied Physics, Electrical Engineering  
Faculty Advisor: Claudio Mazzoleni, Physics

**Introduction:** The study of clouds, atmospheric aerosol, and turbulence is important to understanding the Earth's climate. Temperature is a key parameter regulating the formation of clouds. However, many current measurement methods require some sort of probe which can alter the turbulence of the air. The focus of this research is developing a system to measure atmospheric temperature remotely, exploiting the Raman effect.

**Materials and Methods:** The beam of an easily tunable, but low power laser is directed into the cavity of a second laser. This secondary laser has greater power, but doesn't tune well to a specific wavelength. The beam of the former entering the cavity forces stimulated emission in the secondary laser such that its wavelength will match that of the easily tunable laser. The resultant beam exiting the secondary laser is high power, and precisely tuned. This beam is directed to two concave mirrors to achieve a high number of passes between the two. The high number of passes is used to build more power, and obtain more Raman scattering from the air between the two concave mirrors. The scattered light then passes through an imaging system. Following this, the scattered light passes through the rubidium filter. The lasers are set to 780.024 nm, as this is the wavelength at which rubidium absorbs. The rubidium absorbs light that has been elastically scattered, and light that has been Raman scattered passes unchanged to the spectrograph. From the rotational Raman lines, we can measure the temperature by quantifying the ratio of Raman signals within the rotational anti-stokes branches in N<sub>2</sub> and O<sub>2</sub>.

**Results and Discussion:** It was determined that the low power tunable laser is capable of tuning to the very specific wavelength of rubidium absorption. This was proven through observation of the rubidium with an infrared viewer. The rubidium re-emits isotropically the light that it has absorbed. Thus, the rubidium appears to glow, when seen through the viewer, when the tuned laser beam passes through it. This re-emission was also measured with a photodiode and, comparing its reading to the known absorption spectrum of rubidium, the two were in agreement. Next, it was partially confirmed that the low power laser can cause stimulated emission of a particular wavelength in a secondary laser. Its wavelength shifted when the wavelength of the low power laser was changed. While this has not yet been quantified, it is expected the wavelength of the second laser will be identical to the first. In the future, it is expected that the rubidium will sufficiently remove elastically scattered light from any angle, an advantage over other filtering techniques.

## 20. Evolving Curves with Radial Basis Functions

Student Presenter: Nicholas Olinger, Applied/Computational Mathematics  
Faculty Advisor: Dr. Cecile Piret, Mathematical Sciences

**Introduction:** The modelling of evolving curves can be applied to problems in image segmentation, and computer vision. Modelling curve evolutions involves solving partial differential equations (PDE's) on arbitrary curves. Most conventional methods of solving PDE's numerically involve creating a mesh, which is a network of points and cells subdividing the problem, such as a rectangular grid. The Radial Basis Functions (RBF) method is a meshfree technique for solving PDE's, meaning the data can be scattered anywhere, and the points do not need to be connected. This is useful for curves that have complex geometries.

**Materials and Methods:** The original RBF method, also known as the global RBF method, uses every point in the node distribution, which leads to very accurate solutions, but is also computationally expensive, and can lead to ill-conditioned systems. To get around this, we used the RBF-Finite Difference (RBF-FD) method, which is a stable and computationally cheap algorithm. It is a local method, meaning it only considers nodes in smaller a neighborhood around each node to calculate that weight, rather than all the nodes. This is a trade-off between lower accuracy, but much faster computation and improved conditioning. Even with this algorithm, we still had problems with ill-conditioning on certain problems, so we used Polyharmonic splines as our RBF's to deal with this, which we found to be helpful.

**Results and Discussion:** A basic example of a curve evolution is known as mean curvature flow. This is where each point on the curve moves in its normal direction with a sweep relative to its curvature, a measure of how flat or how bendy an area of a curve is at a given point. We were able to use the RBF-FD method along the polyharmonic splines to calculate the normal vectors and curvatures of the points on an arbitrary curve to high orders of accuracy. The research is still ongoing, and we are currently working on producing simulations of curvature flow using our method that we can compare to benchmark problems using other methods.

# SURF

## 21. In-Service Teaching Rehearsals: Recognizing and Responding to Teachers' Confidence

Student Presenter: Gemma Oliver, Mathematics- Secondary Education  
Faculty Advisor: Dr. John Gruver, Mathematics

**Introduction:** Mathematics teacher education can be challenging to deliver in a way that it makes an impact on teacher's practice. Lampert et al. (2013) argue that situating the knowledge teachers gain in teacher education courses in actual teaching practice can help ensure that the knowledge translates to practice. They have argued for the use of teaching rehearsal, where teachers practice teaching a lesson to peers in a low stakes environment where a mathematics teacher educator (MTE) provides in the moment feedback. While this is a promising instructional technique, little is known about how teachers engage in these rehearsals.

**Materials and Methods:** In the summer of 2017 two MTEs, Dr. Hawthorne and Dr. Gruver, engaged 14 middle school teachers in a week long professional development session. The professional development centered on how to teach a unit on algebraic generalization. During the week, the teachers rehearsed how to teach this unit. In total, there were six different rehearsals taught by six of the 14 participants. I chose three of the participating teachers that I felt best represented the diversity of the group to focus my analysis on. These teachers seemed to engage differently in the rehearsals and the purpose of this research was to characterize this differential participation.

During the rehearsals, the MTEs or the other participants would pause the teaching to discuss particular teaching moves. I analyzed these pauses, attending to the acting teacher's gaze and gestures as well as noting the purpose and topic of the pause. After iteratively viewing these phases, the following questions became salient in terms of characterizing the differences in the teachers' participation: Where does the teacher look for suggestions? And How does she engage with the suggestions?

**Results and Discussion:** The teachers looked to different sources for feedback and engaged with that feedback differently. Teacher A tended to look to peers for feedback and generally accepted that feedback. Teacher B tended to look to the MTEs for feedback. Teacher C looked to both sources for feedback, but also seemed to see herself as a competent contributor.

The main contribution of this research is to conceptualize what it means for teachers to engage in rehearsals confidently. This is significant because MTEs can use these results to better notice teachers' engagement. If an MTE was working with a teacher like Teacher A, they could create opportunities for that teacher to engage more critically with suggestions from others. For example, they could ask the acting teacher what she is thinking about the suggestions her peers have made to prompt her to consider its affordances. If an MTE is working with someone like Teacher B, when the teacher is looking to them for a suggestion, they could turn the question to the rest of the group. Thinking about who the teacher is asking for suggestions and how she is engaging with those suggestions can be helpful as MTEs decides how to facilitate productive engagement.

## 22. Bioactive polydimethylsiloxane surface for optimal human mesenchymal stem cell sheet culture

Student Presenter: David Ross, Biomedical Engineering  
Faculty Advisor: Feng Zhao, Biomedical Engineering

**Introduction:** Human mesenchymal stem cell (hMSC) sheets hold great potential in engineering three-dimensional (3D) tissues for diverse applications. Conventional cell sheet culturing methods employing thermoresponsive surfaces are cost ineffective, and rely heavily on available facilities. In this study, a cost-effective method of grafting was utilized for covalently binding a homogenous collagen I layer on a commonly used polydimethylsiloxane (PDMS) substrate surface in order to improve its cell adhesion as well as the uniformity of the resulting hMSC cell sheet. This technology potentially allows for mass production of hMSC sheets to fulfill the demand of thick hMSC constructs for biomanufacturing applications.

**Materials and Methods:** Four PDMS surface treatment groups were prepared for use in surface and cell interaction characterization. The first two were untreated, and plasma etched in order to act as control samples. The other two were coated with collagen using either the traditional adsorption method, or GA/APTES covalent binding. The surface and bulk properties of the samples were assessed using FTIR, sessile drop testing, and AFM. FTIR was used to assess the chemistry of the samples and quantify the collagen adhered to the surface. Sessile drop testing showed the impact of each treatment on the surface wettability of the sample, which plays a large role in the way the cell interacts with the surface. AFM was performed in order to characterize the surface morphology and roughness of the sample. Following standard culturing of hMSCs samples of each treatment group, the cell-surface interactions were characterized through fluorescent imaging, and dna/gene expression analysis. By analyzing the fluorescent imaging, information about the morphology of the cells and confluence of the cell sheets can be obtained. To analyse the dna/gene expression, DNA assays and qRT-PCR were used to assess how many cells were present on each sample, how those cells were behaving.

**Results and Discussion:** Experimentation showed the covalent binding method had more favorable characteristics. Fluorescent imaging and FTIR showed that more collagen was being incorporated into the covalent binding samples than the adsorption samples, and that the collagen layer was more confluent using the covalent binding method. Sessile drop testing indicated that the control and plasma samples had the highest and lowest contact angles respectively, while the covalent binding samples had a slightly higher contact angle than the adsorption method, indicating slightly higher hydrophobicity. AFM results showed that covalent binding samples had a higher roughness than the adsorption samples indicating a higher presence of collagen. Covalently binding the collagen appears to reduce the obvious cracks in the coating present in adsorption AFM images. Based on the Fluorescent imaging of the cell sheets on each of the sample types it appears that the covalent binding samples resulted in the most uniform and confluent cell sheets. These samples had the highest cell area coverage and also showed less evidence of the cell sheet pulling away from the substrate. DNA assays showed similar DNA amounts in the adsorption and covalent binding samples while covalent samples had much higher adhesion complex expression with little impact on stemness.

## 23. Just and Reasonable? Study of Electricity Rates in Houghton County under the Lens of Energy Justice

Student Presenter: Michael Ryan, Social Sciences  
Faculty Advisor: Roman Sidortsov, Social Sciences

**Introduction:** Residents of Houghton county pay among the highest electricity rates in the country. At \$0.22/kilowatt hour (kWh), it is twice both the Michigan average (\$0.11/kWh) and the national average (\$0.10/kWh) raising concerns about equity and justice.

**Materials and Methods:** This project examines the extent and ways in which key stakeholders (ratepayers, the Michigan Public Service Commission (MPSC), and the Upper Peninsula Power Company [UPPCO]) deem the rates and the ratemaking process just and reasonable. In this study, I review the current policies of the MPSC regarding rate approval, examine the UPPCO rate book, the published document that outlines different categories of ratepayers. I also collect and analyze data through interviews of residential ratepayers and compare their statements to the current policy and rates to determine any discrepancies that suggest energy justice issues.

**Results and Discussion:** There appears to be a gap between what ratepayers want and expect out of their electricity rates, and the current policies of the MPSC in what they deem as just and reasonable rates. To gain a better understanding of if these issues are fundamental to energy justice, I suggest further research that expands the demographic of UPPCO customers to include their entire consumer-base, and addition of different categories of UPPCO ratepayers (residential, commercial, industrial).

**SURF**

## 24. The Neuroprotective Effect of Human Mesenchymal Stem Cells in a Spinal Cord Ischemia Model

Student Presenter: Trevor Simmons, Biomedical Engineering  
Faculty Advisor: Feng Zhao, Biomedical Engineering

**Introduction:** Spinal cord (SC) ischemia makes up 1.2% of all strokes and can lead to tissue necrosis which can be associated with pain or loss of sensation. Clinical treatments for SC ischemia are mainly supportive and preventative, with few regeneration therapies available. Many studies have shown that human mesenchymal stem cell (hMSC) based therapies could be used to rescue neuronal death after ischemia. An in-vitro model of hMSC neuroprotection was developed using chicken dorsal root ganglions.

**Materials and Methods:** Chicken dorsal root ganglions (DRGs) were isolated from E9 chick embryos. Four culture surfaces were generated to study neurite outgrowth. On two of these surfaces, polydimethylsiloxane (PDMS) was used in either the flat or nanopatterned and aligned surface subtype with neural growth medium (NGM). For the other two conditions, glass surface was used with either NGM or alpha modified minimum essential eagle medium (alpha MEM). After DRG extraction, neurites grew in their new surface environment for 3 days. Anoxia (0% oxygen) was used in culture for 30 minutes to model acute anoxia in all surface conditions with or without the presence of hMSCs. The cultures were returned to normoxia for 7 days of culture post-ischemia. Neurite length and number was quantified for all conditions using ImageJ and the simple neurite tracer plugin. Statistical analysis was then performed between conditions using JMP Pro (SAS Institute).

**Results and Discussion:** The presence of hMSCs was found to increase both average neurite length and total neurite number in all conditions. No neurite outgrowth was observed in the flat PDMS, aligned PDMS, or glass with alpha MEM environment without the presence of hMSCs. Average neurite length in the other conditions without hMSCs was found to be  $0.468 \pm 0.141$  mm ( $n = 11$ ) and  $1.02 \pm 0.085$  mm ( $n = 58$ ) for aligned PDMS and glass with neural growth medium, respectively. For conditions with hMSC co-culture, the average neurite lengths were found to be  $0.814 \pm 0.094$  mm ( $n = 20$ ),  $0.751 \pm 0.090$  mm ( $n = 27$ ),  $1.849 \pm 0.052$  mm ( $n = 159$ ), and  $1.07 \pm 0.039$  mm ( $n = 153$ ) for flat PDMS, aligned PDMS, glass with NGM, and glass with alpha MEM respectively. Longest average neurite length and largest neurite number were observed in the glass with NGM conditions with hMSC co-culture. The neuroprotective effect of hMSCs in this model has been clearly demonstrated. This relatively inexpensive in-vitro model could be used in future efforts to analyze the influence of growth factors or detailed mechanisms of hMSC neurite rescue.



## 25. Refining the Purification Process of Histone Proteins

Student Presenter: Erinn Smith, Biochemistry and Molecular Biology

Faculty Advisor: Dr. Martin Thompson, Chemistry

**Introduction:** Histone proteins are essential components of nucleosomes and the fundamental units of chromatin. They provide the positively charged core around which the negatively charged DNA can wrap. Mutations found in histone proteins are deleterious because they alter the interaction with DNA or chromatin remodeling proteins. Recently, it has been found that a mutation in a histone protein H3.3 is correlated with a high proportion of malignant pediatric brain cancers. To study how this mutation leads to oncogenesis, the structural differences between reconstituted nucleosome with and without the H3.3 mutation are being examined. Complementary to the differential structural effects, optimum protein purification methodologies were explored to achieve the high-yield and purity of histone proteins needed for the many sample sets required for rigorous examination.

**Materials and Methods:** Three purification protocols are compared for yield and purity of histone proteins, as well as, time and cost effectiveness. The first purification method uses urea and sonication to break apart cell walls followed by and then centrifugation and a cation exchange column purification to purify the proteins. The second method involves an extra step to apply specialized buffers to isolate fractions that contain the target proteins before breaking apart cell walls with urea and sonication and using a cation exchange column to separate the histones from other cell proteins. The third method uses an ethanol/dry ice bath to both purify the histone and break apart cell walls. The Hhistone H3.3 gene was cloned into the pET28a vector and transformed in expression strains of *E. coli*. Proteins were overexpressed following standard IPTG induction protocol. Kanamycin selection was used throughout cell growth and overexpression procedure. All cells were grown on LBK plates and then transferred to LBK liquid media using standard methods.

**Results and Discussion:** The first and second purification methods both worked well on purifying histone proteins, while the third method was less effective. When comparing methods 1 and 2, the latter worked better in terms of purity, however it is more costly and requires more time due to the additional prep-work. Overall, method 1 was most effective in achieving the necessary quality and yield of histone H3.3 protein, and most cost and time-effective. Consequently, this method is preferred for all histone proteins needed for nucleosome reconstitutions. The next steps are to complete histone protein purifications, preparation of DNA fragment, reconstituting mono-nucleosomes for native and mutant histones and structural comparison studies using Atomic Force Microscopy.

## 26. Characterization of Fe-Mn Alloy Phase Diagram in the Low-Temperature Regime

Student Presenter: Philip Staublin, Materials Science and Engineering  
Faculty Advisor: Dr. Paul Sanders, Materials Science and Engineering

**Introduction:** Fe-Mn alloys have been developed for use in coating aluminum automotive components, to improve wear resistance and emulate friction characteristics of traditional cast iron parts. The structure and phase transformations of an Fe-Mn-Al-Cr-C alloy are investigated. Samples of this alloy treated over long times at low temperatures exhibit phase transformations which are not predicted by current iron-manganese phase diagrams, including spinodal decomposition and precipitation of an Al-rich phase. Spinodal decomposition can cause hardening and embrittlement; thus the ability to predict such a transformation is critical to developing alloys for commercial automotive applications.

**Materials and Methods:** Alloy samples with composition Fe-XMn-4Al-2Cr-0.2C (by weight percent, X=25,30,35,40,45,50) were arc-melted over a chilled copper hearth from elemental components. The samples were solutionized under argon atmosphere at 1150°C for 25 hours, and heat treated in vacuum at 300 and 400°C for 672 hours encapsulated in quartz. The microstructures of the resulting samples were characterized using optical metallography, scanning electron microscopy with energy dispersive spectroscopy, and X-ray diffraction. Density functional theory (DFT) calculations were performed to investigate whether spinodal decomposition of a binary Fe-Mn alloy would be predicted based on first principles. DFT allows calculation of the energy of formation of a given atomic structure without use of empirical data. The energy of formation was calculated for face-centered cubic structures with varying composition of Fe and Mn, and the resulting data was fitted to a Redlich-Kister thermodynamic model for comparison to existing empirical thermodynamic models of the Fe-Mn solid solution system.

**Results and Discussion:** The microstructure of the Fe-Mn samples consists of a face-centered cubic austenitic Fe-Mn solid solution phase as well as a layer containing rod-like precipitates near the edges of the samples. The precipitates, rich in aluminum, were formed during quenching after solutionization and were not significantly altered after heat treatment. The thickness of the layer containing precipitates increases with increasing Mn content. The aluminum precipitates, present in every sample above 25wt%Mn, are currently under investigation to determine their structure and mechanism of formation.

Spinodal decomposition, the segregation of elements into two compositions of the same crystal structure, is observed in the Fe-35wt%Mn sample after heat treatment at 300C. Current phase diagrams instead predict the formation of a body-centered cubic (BCC) phase from the austenitic Fe-Mn solid solution [1]. Density functional theory calculations do not predict decomposition of the binary austenitic Fe-Mn structure, suggesting that the segregation may involve the other alloying elements (Al, Cr, C) rather than Mn. The decomposition may be preferred due to the larger kinetic barrier of nucleation of the predicted BCC equilibrium phase. Improved thermodynamic modeling of this transformation can inform design of an alloy which will provide more stable long-term coating for automotive components.

## 27. The Role of Developmental Genes in the evolution of *Drosophila Guttifera* pigmentation patterns

Student Presenter: David Trine, Biochemistry and Molecular Biology  
Faculty Advisor: Thomas Werner, Biological Sciences

**Introduction:** We are currently researching the *Drosophila guttifera* abdominal pigmentation pattern to understand the role of developmental genes in regulating multiple genes in identical patterns. *D. guttifera* exhibits a striking array of melanin spots and shades including six longitudinal spots and a dorsal midline shade on the abdomen. The genes *tan* (*t*) and *yellow* (*y*) are expressed in identical patterns in the abdominal pigmentation pattern. Similar patterns of co-expression are also found in some human cancer genes. Our understanding of cancer will be furthered by studying the genetic mechanisms responsible for regulating formation of the pigmentation pattern in *D. guttifera*.

**Materials and Methods:** For each candidate regulator gene of *t* and *y*, we collect *D. guttifera* pupae of stages p8-p11. The pupae are then dissected and their abdominal epithelial linings preserved. The abdominal epithelial linings are then incubated with a digoxigenin labeled RNA probe complementary to the mRNA sequence of the tested gene. Unbound probe is rinsed away. Then anti-digoxigenin antibodies with alkaline phosphatase conjugate are added. Once excess antibody is removed, NBT and BCIP are added. NBT and BCIP react in the presence of alkaline phosphatase to form a purple crystalline precipitate. The location where the potential regulator is expressed is indicated by precipitate. Once the pattern of expression is ascertained, the reaction is halted and the epithelial linings are imaged.

**Results and Discussion:** We are currently screening 24 candidate genes for signs of upstream regulation of *t* and *y*. Our prior research located a cis-regulatory element (CRE) in both the *t* and *y* loci that drives expression of the abdominal spot pattern. This research also suggests the spot pattern evolved from a stripe pattern through partial repression by an unidentified repressor. Species closely related to *D. guttifera* show stripes in varying degrees of separation into spots, supporting this repression model. We hypothesize that one of the 24 test genes regulates this repressor's activity in *t* and *y*. If so, purple crystal pattern would be observed in each row between the latitudinal and midline spots and between the midline and dorsal spots. Identifying upstream regulators of *t* and *y* will promote our understanding of how developmental genes regulate the co-expression of multiple target genes.

## 28. Understanding Determinants of Asthma Among Adults in the U.P

Student Presenter: Ayla Vaughn, Biochemistry and Molecular Biology

Faculty Advisor: Dr. Kelly Kamm, Kinesiology/Integrative Physiology

**Introduction:** The WUPHD (Western U.P. Health Department) and partners conducted a health needs assessment in the U.P. to provide region specific data (2017 Health Survey of Upper Peninsula Adults). The state of Michigan conducts similar studies. Upper Peninsula residents are under-represented in these data due to population-based sampling strategies. In the U.S., 18.4 million adults and 6.2 million children have asthma but little research has been done on populations in rural areas, (CDC). I sought to describe adult asthma in the U.P. and identify high-risk groups to inform public health interventions.

**Materials and Methods:** The 2017 Health Survey was modeled after the CDC Behavioral Risk Factor Surveillance System. It was a self-administered survey sent to 23,800 randomly sampled U.P. households in July 2017. This research is a secondary data analysis. The exposures of interest were:

Demographic:

- Age
- Gender
- BMI
- Income
- Education
- County of residence

Health Concerns:

- Smoking status (tobacco and marijuana)
- Drug use
- Health status

Healthcare systems:

- Insurance status
- Access to healthcare

The outcomes of interest were 1) ever vs. never having asthma, 2) currently vs. never having asthma, and 3) currently having asthma vs. formerly having asthma. I will be using bivariate and multivariate logistic regression models using SAS statistical software, University Edition.

**Results and Discussion:** Responses were received from roughly 5000 individuals. Surveys where more than 50% of the responses were blank or where duplicate entries were found were deleted. The final sample size was 4820, an average of 344 surveys per county (range: N=272 Menominee, N=524 Ontonagon). Respondents classified as current, former, or never having asthma differed on currently having asthma being far more likely to be obese compared to never or formerly having asthma. Also women are looking more likely to have asthma compared to men. Data analysis is ongoing at this time.



## 29. The Effects of Cognitive Demands and Stress on Prefrontal Cortex Activation and Motor Unit Variability

Student Presenter: Derek Verbrigghe, Exercise Science  
Faculty Advisor: Tejin Yoon, Kinesiology/Integrative Physiology

**Introduction:** Activities of daily living and work-related tasks often involve simultaneous performance of cognitive and motor tasks. During these tasks, fine motor controls such as steadiness and accuracy are required. Prefrontal Cortex (PFC) roles are particularly important because the PFC may integrate sensations from various sources and send critical information to the motor area of the brain. In this study, we will determine if exposure to a cognitive challenge impairs motor control by increasing the excitability of the motor neuron pool (motor unit discharge variability) and/or increases activation in the PFC during low-force contractions.

**Materials and Methods:** Three healthy young men ( $20.0 \pm 1.0$  years) volunteered for the study. Initially, subjects were screened for physical and neurological health and performed a biometric test. Using a Biodex chair and customized load cell, subjects were positioned and set up for voluntary isometric contractions of their elbow flexors. A dEMG was positioned over the belly of the biceps brachii in order to quantify motor unit variability via the coefficient of variance for interspike intervals (ISI) of the motor units during the tasks. Subjects performed 3 maximum voluntary contractions and had a functional near infrared spectroscopy (fNIRS) device strapped to their forehead in order to measure PFC oxygenation. Subjects had a short familiarization session where they traced a line set at 20% of their MVC. Next, subjects performed the motor task by tracing a line set at 30% of their MVC six times. Then subjects performed the cognitive challenge by completing serial subtractions of 13 from a 4-digit number for three minutes. Lastly, subjects performed both the motor and cognitive tasks simultaneously. An MVC was taken after each motor task to ensure muscle fatigue was limited, and stress, pain, and anxiety questionnaires were taken in between each stage of testing.

**Results and Discussion:** Force fluctuations were greater during the combined task than the motor task ( $2.74 \pm 0.76$  vs.  $3.09 \pm 1.08\%$ ,  $P = 0.05$ ; averaged value of each intensity). 18-61 decomposed motor units at each task were compared, and ISIs during the combined task were lower than ISIs during the motor task ( $23.3 \pm 0.75$  vs.  $22.1 \pm 1.10\%$ ,  $P > 0.05$ ). Also, oxygenation level was similar between both tasks for all channels ( $0.99 \pm 0.36$  vs.  $0.75 \pm 0.80 \mu\text{M}$ ,  $P > 0.05$ ). Force fluctuations and motor unit variability were significantly correlated ( $r^2 = 0.366$ ,  $P < 0.05$ ) and PFC activation was not associated with motor unit variability (all channels,  $P > 0.05$ ). This result may be due to the small sample size of this pilot study or low sensitivity of the dEMG technique. Further research with a larger sample size is warranted.



## 30. Understanding Tubercle Microbial Communities and their Impact On Great Lake Structures

Student Presenter: Paige Webb, Medical Laboratory Science  
Faculty Advisor: Stephen Techtmann, Biological Sciences

**Introduction:** Microbial influenced corrosion is a major cause of corrosion on metal structures in the Great Lakes, and results in both compromised structural integrity and the need to more frequently repair and/or replace these structures. In Duluth Superior Harbor the effects of these microorganisms are felt strongly due to their influence of corroding over 13 miles of steel sheet pile walls in the Duluth Seaway Port, it is estimated to repair this damage it would take between \$90-100 million. This research looks into how iron oxidizing microbial communities are colonizing Great Lakes steel structures and how they may be contributing to the accelerated rusting process.

**Materials and Methods:** Six materials were chosen to study the rate of microbial colonization. These materials were; Stainless Steel, Aluminum, Coated Low-Carbon, General Purpose Low-Carbon, and HDPE was chosen as a control to identify bacteria that are specific for colonization of metals. Six coupons of each material type were deployed near the GLRC dock such that the coupons were near each other. Once every week for six weeks one of the coupons from each material type was collected, cataloged, and processed. In addition to studying the initial steps of colonization, samples were taken from the tubercles already attached to the dock. The microbial communities from the coupons and the tubercles were extracted. The DNA extractions were done using PowerSoil DNA extraction kits from MoBio Laboratories Inc, and followed the protocol of (Oldham, 2016). Abundance of *Gallionella* spp. was determined using qPCR methods as described in (Li et al., 2010). To determine the community composition on the metal coupons, 16S rRNA sequencing was performed according to the protocols described in (Techtmann et al 2015).

**Results and Discussion:** qPCR data showed that in the first week of colonization Eukaryotes and Cyanobacteria composed of 41-81% of organisms growing on the coupons. By the sixth week that number declines to 17-34% of the microbial community that grew on the coupons.

- Concentration of *Gallionella* over time
  - *Gallionella* colonized all of the material types
  - They colonized some materials early and remained at high concentrations throughout.
  - They colonized other materials with increasing numbers and then died off at later points.
- Many of the initial colonizers for some of these metal types are microbial ---
- Eukaryotes followed at later weeks by higher concentrations of bacteria.
- There seems to be a similar community that colonized the coupons regardless of material type.

The data indicates that there is another microorganism that is biofouling the coupons due to the visual examination of the general low-carbon coupon on the sixth week. qPCR data showed that the percent of *Gallionella* declines through the weeks, but on visual inspection of this coupon it is completely corroded indicating that another microorganism could be combined with the iron oxidizer to help in the biofouling that is occurring.

# SURF

# 31. Regional Scale Back-Analysis Using TRIGRS: An Approach to Advance Landslide Hazard Modeling and Prediction in Sparse Data Regions

Student Presenter: Luke Weidner, College of Engineering

Faculty Advisor: Thomas Oommen, Geological and Mining Engineering and Sciences

**Introduction:** In Kerala, India, deadly landslides are triggered by periods of both extreme monsoon precipitation and elevated groundwater levels. Modeling the slope stability is one option to predict when and where landslides could potentially happen, but obtaining the input data required for the slope stability models can be prohibitive, especially in developing countries such as India. By employing various remote sensing techniques, we aim to use the TRIGRS rainfall-induced slope stability model to derive critical information about the causes of previous landslides in a data-poor region. This technique could support the future deployment of landslide early warning systems over large areas.

**Materials and Methods:** A 375 km<sup>2</sup> region was chosen to apply the model, experiencing one failure on June 6, 2004 at 4:00 am and at least 14 failures on July 17, 2007 at 2:00 am. The input files for TRIGRS are slope, soil thickness, rainfall intensity, geotechnical properties of soil, and water table depth. Slope was derived from a 30m resolution Digital Elevation Model (DEM) from the SRTM satellite. Rainfall intensity for the two events was estimated using the Tropical Rainfall Measuring Mission (TRMM), which creates near-real-time precipitation estimates for the tropical latitudes. Comparison of TRMM with ground-based measurements showed close agreement (coefficient of correlation: 0.91). Soil thickness was assumed to vary with the cosine of ground slope. Ranges of soil strength properties (cohesion, friction angle, hydraulic properties) were obtained from previous investigations in Kerala, and water table depth was assumed uniform over the entire area to allow for quick adjustment. For both failure events, cohesion, friction angle, and water table were varied within their ranges until the TRIGRS modeled failure time (time when minimum FS drops to < 1) matched with the actual reported failure time. FS and pore pressure output grids were generated at all time steps for analysis.

**Results and Discussion:** First, back-analysis from the July 2007 event determined cohesion, friction angle, and water table depth values of 1.5 kPa, 34 degrees, and 1.7 meters, respectively. This parameter set was then applied, remarkably without modification, to a forward model of the June 2004 event, and failure time was successfully predicted for this second event (< 5 hours deviation from reported time). Spatially, the total predicted failure area was much larger for the 2007 event than for the 2004 event, in agreement with local reports, but the prediction accuracy was low with a high number of false positives. Being typical of this type of model, this is explained by the low resolution and simplifying assumptions of inputs. The models' equivalence in water table depth suggests both failure events had similar critical groundwater conditions despite vastly different rainfall amounts, which could be useful for anticipation of future failures in this region. The results demonstrate that by using available remote sensing resources, landslide properties can be determined despite data-poor circumstances using TRIGRS. We can also conclude TRIGRS shows potential in predicting failures and provides a valuable tool for the development of early-warning systems in Kerala.

# SURF

## 32. Distributed Manufacturing of Flexible Products: Technical Feasibility and Economic Viability

Student Presenter: Aubrey Woern, Mechanical Engineering

Faculty Advisor: Dr. Joshua Pearce, Materials Science and Engineering

**Introduction:** Distributed manufacturing even at the household level is now well established with the combined use of open source designs and self-replicating rapid prototyper (RepRap) 3D printers. Previous work has shown substantial economic consumer benefits for producing their own polymer products. Now flexible filaments are available at roughly 3 times the cost of more conventional 3D printing materials. To provide some insight into the potential for flexible filament to be both technically feasible and economically viable for distributed digital manufacturing at the consumer level, this study investigates 20 common flexible household products.

**Materials and Methods:** The 3-D printed products were quantified by print time, electrical energy use and filament consumption by mass to determine the cost to fabricate with a commercial RepRap 3D printer. Printed parts were inspected, and when necessary, tested for their targeted application to ensure technical feasibility. Then, the experimentally measured cost to DIY manufacturers was compared to low and high market prices for comparable commercially available products. In addition, the mark-up and potential for long-term price declines was estimated for flexible filaments by converting thermoplastic elastomer (TPE) pellets into filament and reground TPE from a local recycling center into filament using an open source recyclebot.

**Results and Discussion:** This study found that commercial flexible filament is economically as well as technically feasible for providing a means of distributed home-scale manufacturing of flexible products. The results found a 75% savings when compared to the least expensive commercially equivalent products and 92% when compared to high market priced products. Roughly, 160 flexible objects must be substituted to recover the capital costs to print flexible materials. However, as previous work has shown the Lulzbot Mini 3D printer used in this study would provide more than a 100% ROI printing one object a week from hard thermoplastics, the upgrade needed to provide flexible filament capabilities can be accomplished with 37 average substitution flexible prints. This, again easily provides a triple digit return on investment printing one product a week.

**SURF**

